eng

MDPI

Article

Energetic Characterization of Bound Moisture in Faecal Sludges

Arun Kumar Rayavellore Suryakumar [1,*], Larona Malope [1], Sergio Luis Parra-Angarita [2], Angélique Léonard [2], Jonathan Pocock [1,3] and Santiago Septien [1]

[1] WASH R&D Centre, University of KwaZulu-Natal, Durban 4005, South Africa; laronamalope@gmail.com (L.M.); pocockj@ukzn.ac.za (J.P.); septiens@ukzn.ac.za (S.S.)
[2] Chemical Engineering Research Unit, Products, Environment, and Processes, University of Liège, 4000 Liège, Belgium; slparra@uliege.be (S.L.P.-A.); a.leonard@uliege.be (A.L.)
[3] Department of Chemical Engineering, University of KwaZulu-Natal, Durban 4005, South Africa
* Correspondence: 220112475@stu.ukzn.ac.za or rsarunkumar@gmail.com

Abstract

In fecal sludges (FSs) from non-sewered sanitation systems, bound moisture constituted 46–67% of total moisture across all sanitation types investigated, yet the energetic basis for its resistance to removal has not previously been characterized. Existing classifications of moisture fractions lack quantitative binding energy data, leaving the thermodynamic limits of solid–liquid separation undefined for FS. This study investigates the distribution and binding energies of bound moisture fractions in FS obtained from ventilated pit latrines, urine-diverting dehydrating toilets, and septic tank systems. Bound moisture fractions were determined using moisture sorption isotherms, low-temperature convective drying, nuclear magnetic resonance, and thermogravimetric–differential scanning calorimetry analyses. Results show that interstitial moisture constituted 37–50% of total moisture, followed by vicinal (6–14%) and intracellular (3–9%) fractions, with net isosteric heat rising sharply below 20–30% moisture content (w.b.). Evaporation enthalpy exceeded that of bulk water at moisture contents below ~30% (w.b.), consistent with EPS-mediated adsorption and capillary confinement contributing to increased energy requirements for moisture removal and indicating a transition from capillary-controlled to structure-influenced retention. These findings provide a thermodynamic basis for interpreting why conventional mechanical dewatering stalls at a residual moisture content that differs systematically between VIP, UDDT, and septic tank sludges. These insights are relevant for improving FS treatment strategies, particularly in selecting appropriate combinations of dewatering, drying, and pre-treatment processes.

Keywords: fecal sludge; moisture boundness; binding energy; net isosteric heat; sludge dewaterability

Academic Editor: Antonio Gil Bravo

Received: 13 April 2026
Revised: 8 May 2026
Accepted: 18 May 2026
Published: 25 May 2026

1. Introduction

Approximately 70% of households in developing regions rely on non-sewered sanitation systems, making fecal sludge (FS) treatment a critical factor in preventing land and water contamination. Effective FS treatment not only mitigates health and environmental risks but also facilitates the recovery of valuable nutrients and organic matter for beneficial reuse. While solid–liquid separation is typically the first step to reduce volume,

mechanical dewatering is usually employed, with further drying required to achieve safe handling, transport, or resource recovery targets. The transition between these stages is governed by the nature of moisture retained within the sludge matrix [1,2]. However, FS remains insufficiently characterized due to its inherent variability and unpredictability, with moisture content ranging from 60 to 99% across sanitation types [3] making standardized dewatering protocols unreliable [4].

Moisture boundness, defined as the strength of interaction between water and the sludge matrix, is a key factor influencing moisture mobility and resistance to removal in fecal sludge treatment processes. It governs the extent to which moisture can be separated under applied mechanical, thermal, or physicochemical conditions. Effective solid–liquid separation decreases the amount of FS to be transported and, more importantly, reduces the treatment footprint and improves the resource recovery potential of FS treatment products [4]. The moisture content (MC) of FS varies from 99% to 60% depending upon various factors, mainly on the type of onsite sanitation system and the extent of the use of water for anal cleansing [1]. Some of the mechanical solid–liquid separation technologies commonly used include belt press, screw press, filter press, centrifuge press, etc., and the common non-mechanical method adopted is the use of drying beds with or without thermal drying [5,6].

Several studies on sewage sludge have identified parameters influencing solid–liquid separation, with moisture distribution within the sludge matrix emerging as a key factor [7,8]. Among these parameters, the boundness of different types of moisture within the sludge plays a key role in determining the dehydration limits and selecting the most suitable dewatering technology [9,10]. Due to its significance, various authors have proposed classifications for the different moisture fractions in sludge, with the most relevant summarized as follows. Moller (1983) [11] distinguished interspace water, capillary water, adhesion water, adsorption water, and internal water. Smollen (1988) [12,13] classified moisture into free water, immobilized water, bound water, and chemically bound water. Colin and Gaz-bar (1995) [14] proposed a classification including free water, water not removable mechanically, bound water removable under realistic mechanical strain, and bound water removable under extreme mechanical strain. Kopp and Dichtl [15,16], Vesilind, and Vaxelaire [17] (2000; 1997, 2003; 2004) identified free moisture, interstitial moisture, surface (vicinal) moisture, and intracellular (internal) moisture.

From these classifications, the primary categorization of sludge moisture is unbound and bound moisture. While the unbound or free moisture is considered to be the portion of moisture which is able to move freely within the floc structures and thus is relatively easier to remove due to the absence of any binding energies with the sludge particles, the bound moisture has solid to moisture bond strength that binds the moisture to the sludge particles. The bound moisture or immobilized moisture is thus physically or chemically (or both) bound to the solid particles in the sludge. The distinction between unbound and bound moisture provides an operational understanding of the sludge dewaterability limits. However, recent investigations have demonstrated that the transition between these states occurs over a range rather than at a discrete boundary. This overlap arises due to the coexistence of loosely associated bound moisture and tightly retained unbound moisture within the sludge matrix [18]. Consequently, understanding the sludge solid–liquid separation behavior requires moving beyond the fraction-based classification towards quantifying the energetic interactions governing moisture–particle association. To facilitate the interpretation of the different moisture fractions and their spatial distribution within the sludge matrix, a schematic representation is provided in Figure 1. This visualization complements the previous textual description by illustrating the location and interaction of interstitial, vicinal, and intracellular moisture within the biofloc structure.

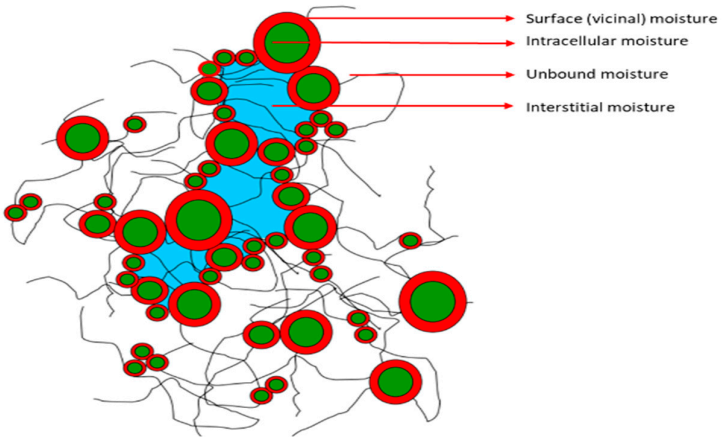

Figure 1. Schematic representation of moisture boundness in the microspatial structure of solid bioflocs, illustrating interstitial (blue), vicinal(red), and intracellular (green) moisture fractions [19,20].

The total bound moisture is the sum of interstitial moisture, vicinal moisture and internal moisture. As illustrated in Figure 1, the interstitial moisture is trapped between the sludge flocs and, since the moisture is trapped between the flocs, no direct forces are acting on the moisture [10]. However, experiments have shown that it is bound by weak active capillary forces. Also, osmotic pressure within the sludge flocs is another force which acts on interstitial moisture [21]. The vicinal moisture or surface moisture is bound by adsorptive and adhesive forces and can be separated only by disintegrating the floc or disrupting the cell. The vicinal moisture is bound physically to solid particles and cannot be removed by mechanical forces. The internal moisture is contained within the cell bodies and is biochemically bound to the solid particles [15].

Thermodynamically, the bound moisture does not behave as pure water, as the chemical potential and binding strength are naturally different from that of pure water [22]. The interstitial and the vicinal moisture, because of the solid flocs and high dissolved solids concentration, freezes at a temperature lower than the normal freezing temperature of water, with the vicinal moisture freezing at very low temperatures. The intracellular moisture does not enter the ice crystal lattice upon freezing. It can only be removed thermally above 105 °C [17,18,23]. The removal of bound moisture involves overcoming these respective binding strengths of the moisture with the solid particles.

Although bound moisture fractions have been previously reported for sewage and industrial sludges, limited understanding exists regarding how these fractions relate to progressively increasing binding energies and their implications for moisture mobility and removal mechanisms. Specifically, in FS, characterized by the heterogeneous biofloc structures with extracellular polymeric substances (EPSs), the energetic hierarchy of moisture binding remains largely unexplored. Establishing this hierarchy is essential to explain the dewatering processes which remove certain moisture fractions while others remain resistant despite increased applied stress.

Following the experimental identification of the unbound–bound moisture interface [18], the present research investigates the internal structure of the bound moisture domain by determining the distribution of the bound moisture fractions, together with their corresponding binding energies. In this study, the moisture boundness considered is based on the type of interaction of the water molecules with the solid biofloc structures (Figure 1) and accordingly, the bound moisture is categorized into three types based on the extent of the solid to moisture bond strength as per [17,19,23,24], namely interstitial moisture, vicinal moisture and intracellular moisture.

The extent of the total bound moisture is reliably revealed by different techniques and instruments such as water activity measurement (WA), differential scanning calorimetry (DSC) and thermogravimetric analysis (TGA) [18]. It is the bound water fractions which are not well known. These fractions, along with the stabilized aggregation of microbes as colloids, influence the selection of technologies for solid–liquid separation [25,,26]. To fully understand the mechanisms of moisture boundness and to consider the types of pre-treatments associated with solid–liquid separation to convert bound moisture to unbound, the knowledge of the proportions of all types of bound moisture is a pre-requisite [27,28]. Since there are different types of binding forces, the removal of different types of bound moisture could require different approaches. Thus, determining the proportions of the bound moisture fractions will help in their conversion to unbound moisture, by appropriate technologies [29]. Along with quantifying the proportions of bound moisture fractions, the objective is also to characterize the associated binding energies using thermodynamic and sorption-based approaches. By linking moisture fractions to their associated energetic requirements, this work provides an empirical basis for interpreting the relationships between moisture boundness, physicochemical binding, and sludge solid–liquid separability behavior. While this study does not directly evaluate specific technologies, it provides a basis for interpreting why different treatment approaches perform differently depending on the dominant moisture binding regime.

2. Materials and Methods

2.1. Source of Samples

FS samples were collected from eThekwini municipality, Durban, South Africa and from the peri-urban areas of Pietermaritzburg, South Africa and included samples from different onsite sanitation systems, namely:

1. Ventilated pit latrines (VIPs);
2. Urine diversion dehydrating toilets (UDDTs);
3. Septic tanks (STs) (also referred to as septage):
    a. With grey water (ST-wGW);
    b. With only black water (ST-BW).

The VIP samples were collected from two latrines not desludged for at least 5 years. The UDDT samples were taken from the dehydrating vault of the UDDT, with an estimated sludge storage of 15–18 months. The septic tank samples were collected from the desludging vacuum tanker trucks, and composite samples were taken from septic tanks which are connected only to the toilets (ST-BW) and the ones connected to all the wastewater flow (ST-wGW). The desludging interval of STs was usually a year for ST-wGW and 4–6 years for ST-BW. All the samples were collected in lined plastic containers with air-tight lids from the peri-urban areas within the jurisdiction of eThekwini municipality, Durban. All the samples were screened for trash and debris removal and stored in the cold room at the laboratory at 4 °C to avoid microbial degradation and to minimize any loss of moisture. The samples were analyzed for total solids (TS), volatile solids (VS), pH and electrical conductivity (EC) at the time of sampling, and these parameters were monitored for any change during the experimental period. Variation in the parameters was found to be within the acceptable range of <5%. The physical, mechanical and textural properties of FS and its influence on moisture boundness have been previously documented [20]. Ethical clearance was obtained for this research from the Biomedical Research Ethics Administration (BREC) from the University of KwaZulu-Natal (protocol reference number: BREC/00002194/2020).

2.2. Experimental Methods

2.2.1. Moisture Vapour Sorption

The relationship of moisture content as a function of relative humidity, at a given temperature, is one of the important aspects of moisture boundness. Given by moisture sorption isotherms (MSIs), this describes the amount of moisture adsorbed or desorbed at equilibrium for a given temperature. Most MSIs have a sigmoidal shape and can be divided into three regions, as shown in Figure 2. Zone 1 represents a monolayer, where moisture is strongly associated with the solid material, and corresponds to tightly bound vicinal moisture and all internal moisture. Zone 2 represents a multilayer, and moisture is slightly mobile in this zone, thereby representing most of the interstitial moisture and some loosely bound vicinal moisture. Zone 3 represents unbound moisture [21,22].

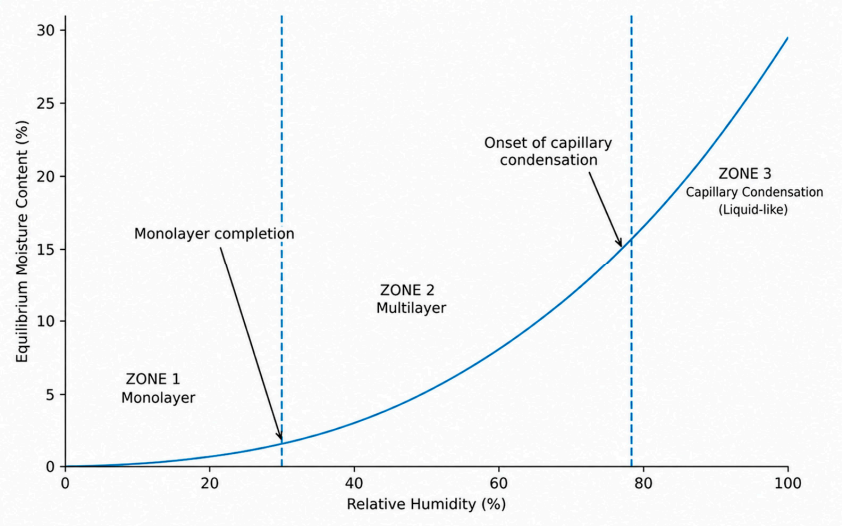

Figure 2. Generalized moisture sorption isotherm, with its three regions, with first transition point indicating completion of monolayer adsorption, and the second transition point indicating the onset of capillary condensation [30].

MSI experiments were conducted by three different methods—water activity measurement, dynamic vapor sorption and the saturated salt solution method.

Water Activity Measurement

Commonly used in the food industry for food safety and quality, water activity measures the state of moisture in the organic matter. It is a measure of the thermodynamic activity of water vs. the moisture content in the sludge, at a given temperature. As a function of moisture content, it is a good indicator of the boundness of moisture with the solid particles [18]. The samples were dried in an oven at 105 °C for different pre-defined intervals and the corresponding water activity measurement was carried out with an AquaLab Tunable Diode Laser (TDL) water activity meter (Meter Group, Pullman, WA, USA). This spectroscopic method measures by absorption at a wavelength of 1854 nm when laser light is transmitted through the headspace atmosphere above the sample which is placed in a sealed chamber. The temperature was set to 22 °C, with a resolution of ±0.0001 and accuracy of ±0.005. All samples were measured in triplicates [25]. After determining the water activity, the samples' MC was measured using a Radwag Max 50 Thermal Moisture Analyzer instrument (RADWAG, Radom, Poland).

Dynamic Vapor Sorption

The dynamic vapor sorption instrument (DVS Intrinsic, Surface Measurement Systems, London, UK) utilizes divided flow technology by varying the relative humidity (RH). Dynamic vapor sorption (DVS) works on the principle of gravimetric sorption and measures how quickly a solvent is absorbed by the sample. This is done by varying the vapor concentration in the surrounding gas and measuring the change in the mass of the sample. DVS is employed in various sectors to study compound stability and surface sorption effects of moisture and other organic vapors. DVS is programmed to cycle between different humidity levels and measures the uptake or loss of moisture by a carrier gas (nitrogen) flowing over the sample, which is suspended on a microbalance, and keeps the humidity constant until the equilibrium mass is achieved. This technology generates the MSI in a relatively short period of time [22]. Further, for the dynamic sorption method, the equilibrium criteria are not as severe as for the saturated salt solution method, and the sorption isotherm can be obtained relatively quickly, in a few days, compared to a few weeks using the static method [26].

The DVS instrument was used to determine the dynamic sorption isotherms at the Chemical Engineering Laboratory, the University of Liège, Belgium. The FS samples were about 15–25 mg and loaded onto the sample pan. Two sorption–desorption cycles were used in this work—from 0% to 90% air relative humidity (RH) and back to 0% RH, and from 90% to 0% RH and back to 90% RH. The incremental step was 10% RH. The samples were maintained at a constant RH until the mass variation per minute (dm/dt) was <0.0015% for 10 min. The experimental results were recorded in terms of the change in the sample mass as a function of time for consecutive RH values as defined by the sorption cycles. All the experiments were conducted at 40 °C. Calibration was performed prior to each experimental run to stabilize the temperature and relative humidity conditions.

The raw samples were analyzed using the DVS Standard Analysis System, which allowed the construction of hysteresis curves [27]. The equilibrium moisture contents (M_{eq}) were determined at the different RHs from 90% to 0% and 0% to 90%.

Static Gravimetric Method

The traditional approach of using saturated salt slurry to determine the MSI was carried out at different temperatures. The method involved placing the sludge sample in a jar with a saturated salt solution of known RH in closed containers and measuring the weight of the sample until there was no change in the weight of the sample. The saturated salt solutions were prepared at pre-determined concentrations in Mason jars, with the salt mixed with distilled water until excess crystals were formed. Eight saturated salt solutions were prepared corresponding to different RH values, from 8.9% to 94.1% (Table 1) [28].

Table 1. Relative humidity obtained for the different saturated salt solutions.

Saturated Salt Solutions	RH at 20 °C
Potassium Hydroxide (KOH)	9.3%
Sodium Hydroxide (NaOH)	8.9%
Calcium Chloride ($CaCl_2$)	28.8%
Magnesium Nitrate ($Mg(NO_3)_2$)	54.4%
Cupric Chloride ($CuCl_2$)	68%
Potassium Iodide (KI)	69%
Ammonium Sulfate ($(NH_4)_2SO_4$)	80.0%
Potassium Nitrate (KNO_3)	94.1%

The FS samples were homogenized manually, and 1.5 g of VIP and UDDT samples and 3 g of ST samples were placed in 100 mL saturated salt solution jars of different RHs.

The samples were continuously weighed using an analytical balance until no change in the weight was recorded. Each experiment ran for a duration of about 2 weeks. A drying oven was used to create the different temperature conditions. All these experiments were carried out in triplicates, and the statistical analysis of isotherm data was determined using relative standard error (RSE), the root mean squared error (RMSE) and mean absolute percentage error (MAPE) [29].

2.2.2. Low-Temperature Convective Drying Tests

The use of drying tests is one of the classical methods adopted for determining moisture content and to determine each fraction of the moisture [31]. The process of drying involves heat and mass transfer between a hygroscopic material and the drying air, with the gaseous medium providing the evaporation heat. The transport of moisture within the sludge occurs due to various mechanisms, with surface diffusion and hydrostatic pressure differences being of interest in the convective drying test [32].

The drying test was first proposed by K. R. Tsang and P. A. Vesilind, 1990 [33], to derive the moisture distribution from the drying curve. The approach assumes different rates of evaporation which indicate the type of bonding between the moisture and the sludge solid particles, thus showing the different phases of drying. Further, the phases of the drying curve are distinct at low drying rates, and hence the experimental set up at the University of Liège was used.

This low-temperature convective drying testing (low-T) was carried out in the test rig for convective microdrying and was designed to handle sludge samples between 5 g to 20 g as shown in Figure 3. The samples were extruded in a circular die of 18 ± 1 mm in diameter and cut at a height of 10 ± 1 mm, with a mass of 5.7 ± 0.2 g. The sample was placed in the drying chamber and subjected to drying at 40 °C, with a superficial air velocity of 3 m/s and fixed absolute humidity at 0.005 kg $H_2O/kg_{dry\ air}$, and was suspended by a supporting grid, connecting to a precision mass balance (Sartorius, Göttingen, Germany). The balance was connected to the computer, and the sample mass was recorded every 5 s. Detailed information regarding the microdryer can be found in a previous study [30]. Compressed air was fed into the system, which was heated to the pre-set temperature before entering the drying chamber. Low-temperature drying at 40 °C was carried out for all the samples. The drying air velocity was controlled with a pneumatic valve.

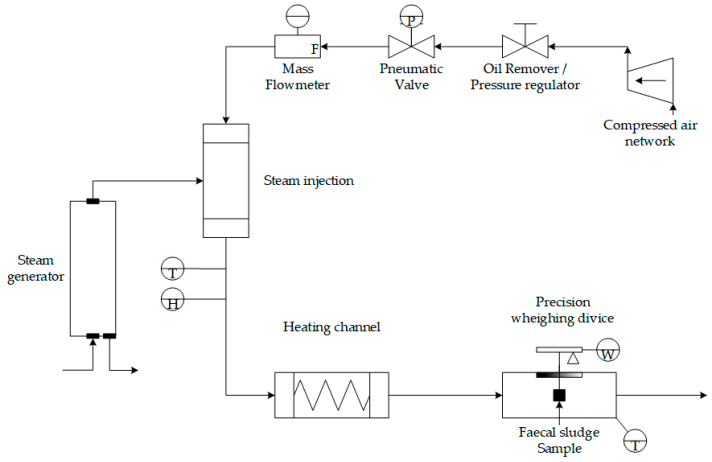

Figure 3. The schematic representation of the convective drying test rig [34].

During drying the FS suffers a shrinkage phenomenon (reduction of the area and the volume), changing the effective transfer area of drying, as show in Figure 4, which affects the drying flux and drying curve. In order to add this correction to the final drying curve,

a methodology was created to follow the area and volume of FS during the drying test [35]. For this, Skyscan-1074 tomography (Skyscan, Aartselaar, Belgium) was used to capture the imagery at different time intervals of low-T convective drying in the microdrying test rig. The tomography operates with an X-ray source at 40 kV and 1 mA, and the detector is a 2-dimensional, 768 × 576 pixel, 8-bit X-ray camera with a spatial resolution of 41 μm.

The *MC* of the samples was calculated according to the following equation:

$$MC = 100\% \times (W_1 - W_2)/W_1 \quad (1)$$

where *MC* is the water content of sludge in %, W_1 is the mass of wet sludge in g, and W_2 is the mass of sludge in g when dried to constant weight at 105 °C [17]. Drying flux was calculated by normalizing mass loss with respect to the instantaneous external surface area, accounting for shrinkage during drying. The plot of drying flux versus moisture is the drying curve, also known as Krischer's curve (Figure 5), and helps to understand the changes in drying rate that correspond to different moisture fractions. A typical drying curve is divided into three sections. The first section after the initial warm up or ramp up phase of the test sample is the constant drying flux period, where the equivalence between heat and mass transfer occurs. This occurs since there is always a film of unbound moisture available at the evaporating surface. The constant drying rate period reflects the extent of unbound moisture in the sample. The constant rate period continues until the compressive strength of the sludge structure becomes lesser than the capillary pressure [36]. The end point of the constant drying rate period is the point of critical moisture, and this corresponds to the limit of unbound moisture or the unbound–bound moisture interface. Though it is regarded as a transition point, this is not always the case. From the previous study [18], the interface is not a single point but a range since the moisture boundness is influenced by multiple factors. Hence, overlap can be factored in, at all transition points. Post the critical MC, the drying surface becomes unsaturated since the migration of moisture to the surface is affected due to internal transport limitations. This is the falling drying rate period, further classified into first falling rate and second falling rate periods, corresponding to interstitial moisture and vicinal moisture respectively [37]. The second critical point X_2 represents the transition from the first falling rate period to the second falling rate period. During the first falling rate period, there is a continuous flow of moisture in the pores, and during the second falling rate period, the movement of moisture in the pores is mainly due to vapor diffusion. Further, as mentioned earlier, this transition point depends on the method of drying adopted and does not necessarily reflect the intrinsic moisture binding characteristic of the sludge material [38].

The drying rate of the samples was calculated using the following equation:

$$DR = (M_{t+dt} - M_t)/dt \quad (2)$$

where *DR* is the drying flux ($kg_{H2O}/m^2 \cdot s$), M_t and M_{t+dt} are the moisture content at time t and $t + dt$ in kg_{H2O}/kg_{TS} respectively.

Sludges are soft materials with mechanical properties governing their solid–liquid separability. Especially during the drying process, shrinkage and crack formation occur due to non-uniform drying and mechanical stress, which influence and alter the drying behavior [39]. We simultaneously measured shrinkage and crack formation using a Skyscan-1074 X-ray scanner (Figure 4). The samples were removed from the drying chamber at pre-defined periodicity and placed in the microtomographic device in order to gain images of several cross-sections, and then the samples were placed back in the drying chamber. The sample height was kept at 1 cm and the sample could be rotated in the horizontal plane and moved in the vertical plane. This helped in getting 2D scans at

different positions [39]. The drying interruptions have been observed to have no significant influence on the drying kinetics [40].

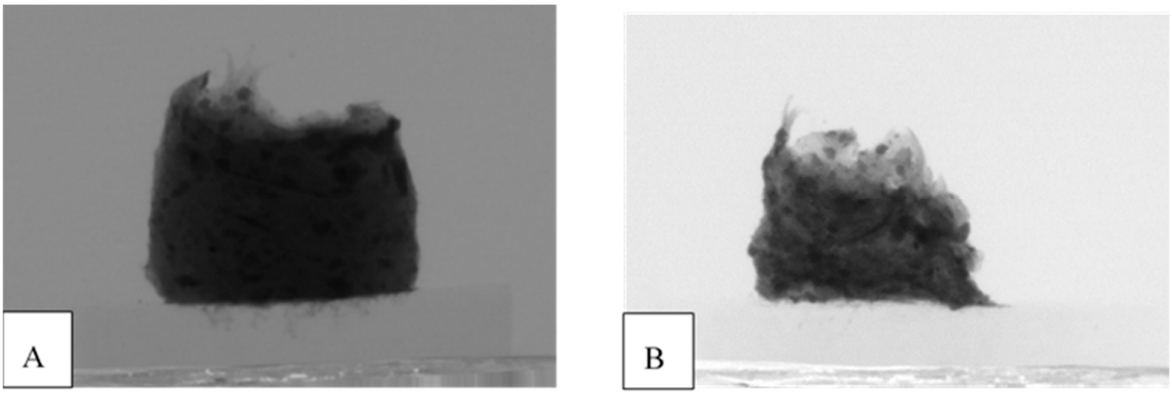

Figure 4. FS shrinkage phenomenon ((**A**)—Before drying; (**B**)—After 220 min of drying).

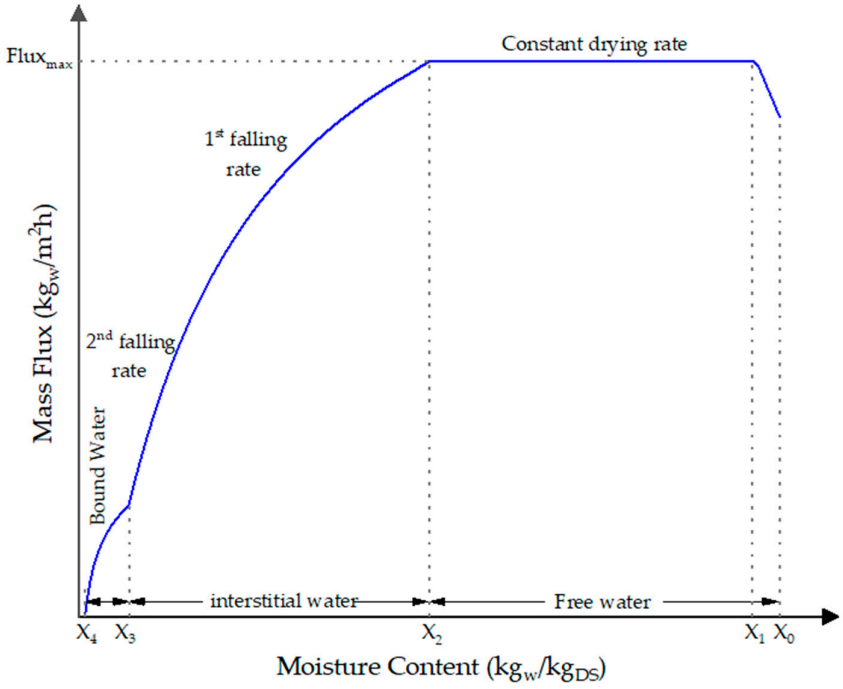

Figure 5. Theoretical drying flux period. In figure 5 The first period, or the preheating period [Xo–X1], represents a period of adaptation of the sample to the drying conditions. The second period, or the constant-flux period [X1–X2], represents the interval during the supplied heat which serves essentially to evaporate the sludge-free water. The third period, or the first falling-flux period [X2–X3], cor-responds to the interval in which the heat serves to evaporate the interstitial water and heat the sludge. The final period, or a second falling-flux period [X3–X4], corresponds to the end of the drying; in this period, the heat evaporates the bound water

The 2-D vertical and horizontal cross-section images were processed and analyzed with the visualization software provided by Skyscan and NRecon. Construction of 3-D images was achieved by stacking of the 2-D cross-section images. Shrinkage was determined by measuring the height and diameter at different drying intervals, resulting in sample volume reduction [40]. The quality of the resulting image was influenced by the quantity of acquired data, and its improvement was directly proportional to the number of projections captured.

Subsequently, MATLAB software, release 2023 was employed for the analysis of the microtomography-derived images and their conversion into mathematical data suitable for generating Krischer's representation. Figure 6 shows from left to right the raw images obtained from tomography, a transversal cut obtained from Nrecon software (V1.7.4.2) and finally a processed black and white image from MATLAB.

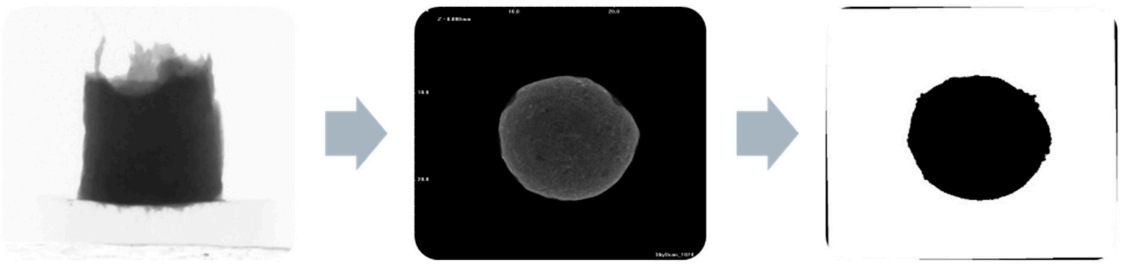

Figure 6. Images before and after processing.

During each interruption of the drying process, the average equivalent diameter (deq, mm) and average height (h, mm) were determined and utilized to calculate the surface area of the sample. In this study, the sludge samples were assumed to be perfect cylinders with their entire surfaces in contact with the drying air.

From low-T test results, Krischer's curve and the soil water characteristic curve (SWCC) were calculated and plotted. The soil water characteristic curve (SWCC) or the soil water retention curve (SWRC) is essential for determining the properties of unsaturated soils and their behavior. Direct measurement of unsaturated soil properties is complex, expensive and time consuming. Hence, researchers suggest the use of saturated soil properties to determine the unsaturated soil properties and thus the use of the SWCC. The application of the SWCC is not intended to imply equivalence between sludge and soil systems, rather it is to provide a mathematical representation of moisture retention behavior under unsaturated conditions, using the van Genuchten model.

Like unsaturated soils, FS is a three-phase matrix of solid particles, moisture and air. This interaction of solid, moisture and air develops a complex energy state, which binds the moisture to the solid particles. The soil suction or the negative pore water potential represents the amount of energy required to expel moisture from the solid matrix in soils. This suction, defined by pF, denotes the logarithm of negative pore water potential and was equated to the drying rate from the low-T drying test of FS, and the moisture retention curve could be obtained by calculating the ratio of drying rate to moisture content of FS [41].

The determination of the SWRC by plotting the volumetric moisture content and soil suction was the essential step towards the characterization of unsaturated soils. The characteristic features of the SWRC are the phase change—denoted by α—which was the air-entry point, the linearity denoted by n, and the infection point m. Thus, amongst the various approaches proposed for mathematical representation of the SWRC, the most commonly adopted model is that developed by van Genuchten [42]. Van Genuchten provided a three-parameter expression for moisture boundness in unsaturated soil hydraulics that is provided by:

$$\Theta = \frac{\theta - \theta_r}{\theta_s - \theta_r} = \left[\frac{1}{1 + (\alpha\psi)^n}\right]^m \quad (3)$$

where θ is the normalized moisture content, ψ is the matrix potential, and s and r are saturated and residual values of moisture content θ respectively.

Soil suction, from the physics point of view, is negative pore water pressure or, in short, capillary rise. Soil suction is when the water content decreases in a natural way, i.e.,

land surface heating up due to solar heat, then the negative water head develops and that is described by the van Genuchten (vG) equation. Here the independent parameter is moisture content [43]. As the moisture content reduced in the soil, from its state of saturation, the point of exposure of the soil particles to air is denoted as the air-entry value (AEV). At this point, air enters the soil pores and is the beginning of the desaturation where the moisture is distributed between the soil particles and adheres to the soil surfaces. As the natural drying continues, the soil suction continues to reduce, and the moisture is removed to a point where the adhesion between the moisture particles is broken, and what remains is the surface moisture, denoted as the residual moisture content. No increase in suction results in any significant change of moisture content beyond this point [34]. The SWRC can thus be categorized into two phases—a stable high-suction region and a rapidly evolving low-suction region since the moisture occupying the micropores lie within the suction range of 0–100 Mpa [44].

Similarly, in the drying test, the moisture removal is by artificially heating up the sample at a low constant temperature. Hence, the independent parameter is the drying rate not the moisture content. By incorporating the inverse of the drying rate (DR), a similar pattern in data behavior is observed, and hence, the application of the same equation can be made to investigate the different types of moisture content.

Thus, adopting the vG equation for sludge, the equation is:

$$\Theta = \theta_r + (\theta_s - \theta_r) / \left[1 + (\frac{\alpha}{DR})^n\right]^m \quad (4)$$

where ψ (soil suction) is replaced by $1/DR$, α, m and n are parameters of the vG equation.

An extended van Genuchten (vG) model was developed to quantitatively characterize the different types of moisture in the FS samples, using the isothermal drying data from the low-T convective drying test. The developed model provided a predictive model for the water retention curve (shown in Figure 7) by calculating the water boundness mechanism of the sludge at micro and macro scales. The main drying data related to the MC of the samples seemed to converge to an inversely proportional curve in a θ (moisture content) vs. drying rate (DR) curve. When the drying approaches infinity, the MC reaches its lowest limit, called the residual water content [42].

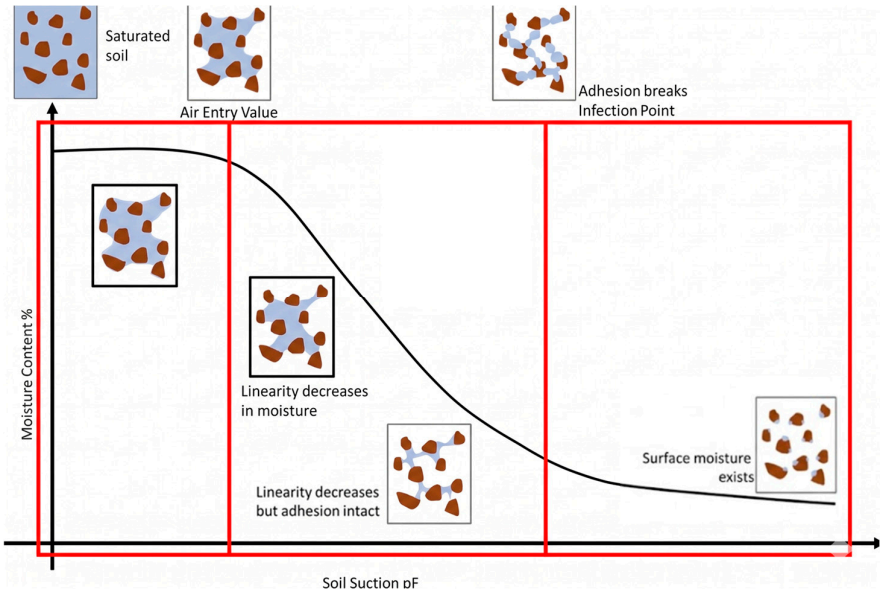

Figure 7. Soil water retention curve—salient features.

2.2.3. Nuclear Magnetic Resonance

Low-field time-domain NMR has been applied to characterize moisture mobility in sewage sludge and porous biological materials, where water molecules in different microstructural environments exhibit distinct T_2 values [45, 46] . Shorter T_2 values correspond to stronger water–solid interactions [47]. In sludge systems, water molecules located in different microstructural environments exhibit distinct transverse relaxation times (T_2), allowing differentiation between loosely bound and tightly bound moisture fractions. Previous studies have applied NMR to investigate moisture mobility in sewage sludge, biological gels and porous biomaterials, demonstrating that shorter relaxation times correspond to stronger interactions between water molecules and solid matrices. Analysis of the T_2 relaxation curves identified different peaks which represented weakly bound and tightly bound moisture fractions [48] with the NMR providing direct insight into the molecular mobility of water within the sludge microstructure.

A Bruker Avance III 500 MHz NMR spectrometer (Bruker Biospin, Ettlingen, Germany) operating at a Larmor frequency of 500.13 MHz (11.75 T) at the University of Swansea was used in conjunction with a Bruker broadband observe (BBO) high-resolution solution probe. Standard 5 mm diameter NMR tubes (Norell S 5-400-7, North Carolina, USA) were used. A sample volume of 200 µL guaranteed that the entire sample was inside the active space of the radiofrequency coils from the BBO probe. The parameter settings used were as follows: the 1H T_2 relaxation curve of the samples was measured with TD-NMR using a Bruker minispec mq20 instrument (Bruker BioSpin, Billerica, MA, USA) at a 1 H frequency of 20 MHz at 25 °C without dilution. One-shot T_2 data was acquired using a standard Carr–Purcell–Meiboom–Gill (CPMG) sequence developed in the 1950s. The acquisition parameters were as follows: number of scans = 8, time between each pulse (τ spacing) = 3.5 ms, total echoes = 3000, recycle delay = 11 s, and dummy shot = 1 [46,47].

The experimental approach undertaken to determine the MC was to use deuterium dioxide 1H ion release to measure the relaxation data. A series of trials with different combinations of the sample and D_2O were conducted. The final experiment is described below, from which we obtained the relaxation data. The samples were not dried nor diluted with distilled water. The TS of the samples were: VIP—24.359%, UDDT—28.345%, ST-BW—8.084% and ST-wGW—1.227% at the time of carrying out the experiments. The relaxation data was obtained when 10–12 g of the raw sample was added to 30 mL of D_2O in a 45 mL centrifuge tube, mixed well, and pipetted into standard 5 mm diameter NMR tubes.

The T_2 relaxation time (T_2) was calculated from the relaxation curves according to a single-exponential curve fitting:

$$M(t) = M_0\left(-\frac{t}{T_2}\right) \quad (5)$$

where $M(t)$ and M_0 are the transverse magnetizations at times t and 0, with a single-exponential decay, respectively at the T_2 relaxation time.

2.2.4. Thermogravimetric Analysis–Differential Scanning Calorimetry (TGA-DSC) Test

The TG-DSC was carried out using a differential thermal analysis–thermogravimetric analyzer SDT Q600 instrument (TA Instruments, New Castle, DE, USA) at the Thermal Analysis Laboratory, Department of Mechanical Engineering, Durban University of Technology, Durban, South Africa, following the methodology proposed by Ferrasse et al. [48,49]. Approximately 35–40 mg of homogenized sample was placed in a ceramic pan, with an empty pan used as a reference. The analysis was conducted under a nitrogen atmosphere (N_2) at a controlled flow rate of 10 mL/min, ensuring an inert environment to prevent oxidative reactions. Samples were heated from ambient temperature (~20 °C) to

90 °C at a constant rate of 10 °C/min, followed by an isothermal holding period of 45 min. All measurements were performed in duplicate.

During heating, the continuous mass loss recorded by TGA corresponds to moisture removal, while the DSC signal provides the associated heat flow. This simultaneous measurement enables differentiation between moisture evaporation and other thermal events and allows estimation of moisture binding strength based on the energy required for evaporation [50]. Thus, the DTA-DSC tests provide the solid particle–moisture binding strength and the residual moisture content is measured continuously and reliably [51,52].

3. Results and Discussion

All experiments were conducted in triplicate, and variability was assessed using standard statistical indicators (RSE, RMSE, and MAPE for MSI data). The observed variability remained within acceptable limits (<5% for key measured parameters), indicating good repeatability across methods.

3.1. Bound Moisture Fractions

3.1.1. Moisture Sorption Isotherms

The moisture vapor sorption experiments were conducted in a water activity meter, DVS and by the saturated salts solution method for all the FS samples. While the DVS and the saturated salt solutions methods provide the moisture content vs. relative humidity, the [51,52] relative humidity is equal to the water activity measurement at the thermodynamic equilibrium. The plot of moisture content as a function of water activity provides different slopes for the different moisture fractions, as shown in Figure 8. In the unbound moisture stage, the water activity remains almost equal to 1. A gentle fall in the water activity below 0.95 indicates the removal of bound moisture, beginning with the interstitial moisture. As the moisture boundness increases, the water activity falls from 0.9 to 0.15, indicating reduction of vicinal moisture. Finally, at a very low moisture content, the water activity is less than 0.1, indicating the presence of internal moisture. This distribution of moisture is shown in Figure 9.

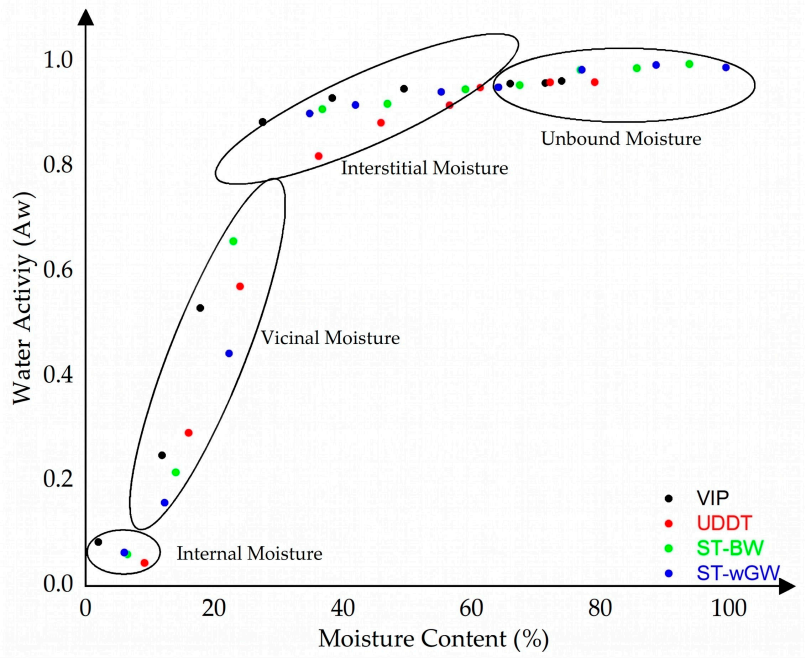

Figure 8. Moisture sorption isotherm from water activity meter of FS samples.

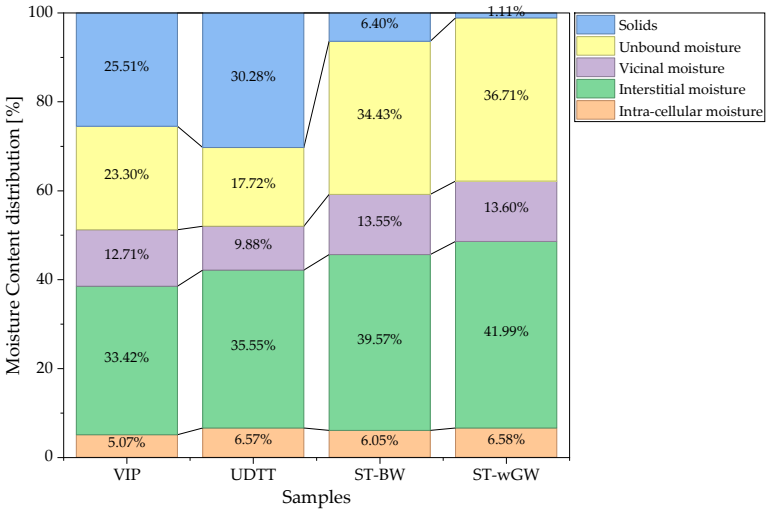

Figure 9. Moisture fractions in the FS samples.

From the dynamic sorption isotherms, the MSI curves resembled the type II sigmoid shape when the MC of the samples was plotted as a function of relative humidity (aw) at a constant temperature. The type II sorption isotherm represents interaction between the material surface and water molecules and is commonly observed in amorphous food types like starch and carbohydrates [22], as observed by other researchers for products with a similar structure [53]. The desorption and adsorption isotherms for the two sorption cycles—90–0%–90% and 0%–90%–0%—were analyzed for the equilibrium MC at the respective RH.

The sigmoidal shape of the MSI curves shows that moisture removal occurs through progressively changing moisture–solid interactions rather than a discrete phase transition. At high water activity, moisture is weakly associated, whereas below $a_w \approx 0.9$, the increasing slope reflects stronger retention, corresponding to the transition toward vicinal moisture. These observations are consistent with a continuous spectrum of binding states rather than abrupt phase boundaries. The transition observed in the MSI curves is consistent with the air-entry behavior described by the van Genuchten model, where similar moisture thresholds indicate the onset of capillary desaturation.

From the literature, The Ferro-Fontan and Peleg models have been previously applied to describe type II sorption isotherms in biological and food materials [21,22]. Both models were selected on the basis of their ability to represent sorption behavior across a wide water activity range. Their performance was evaluated against statistical criteria including RSE, RMSE, and MAPE to confirm their suitability for FS.

The selected models were fitted to the experimental data and evaluated using statistical performance indicators, including the relative standard error (RSE), root mean squared error (RMSE), and mean absolute percentage error (MAPE), as presented in Table 2. As represented in Figure 10, both models provided a good representation of the experimental isotherms across the full range of water activity, with low error values indicating strong agreement between predicted and measured moisture contents.

The ability of these models to accurately represent sorption behavior across both low and high water activity ranges supports their use in characterizing the distribution of bound moisture fractions in FS, particularly in distinguishing between monolayer and multilayer moisture regimes. The sigmoidal nature of the fitted isotherms confirms the presence of distinct moisture binding regimes within the sludge matrix [40].

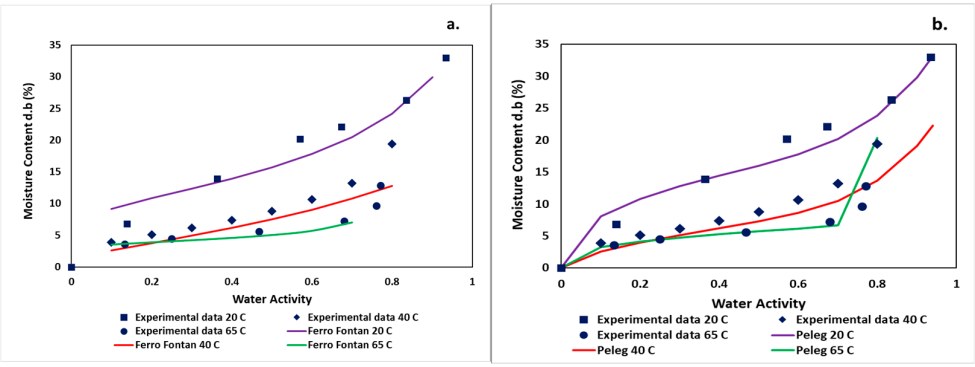

Figure 10. (**a**) Ferro-Fontan model, (**b**) Peleg model fit to VIP experimental data at different temperatures.

Table 2. Error criterion for model validation of the Ferro-Fontan and Peleg models in the FS sample at different temperatures.

Temperature		20 °C			40 °C			65 °C		
Model	**Water Activity**	**MAPE %**	**RSE**	**RMSE**	**MAPE %**	**RSE**	**RMSE**	**MAPE %**	**RSE**	**RMSE**
FF	0.1–0.9	5.23	0.0112	0.0079	1.8553	0.0021	0.0017	7.16	0.0066	0.0046
Peleg	<0.95	3.68	0.0096	0.0068	1.2236	0.0028	0.0021	8.50	0.0179	0.0146

Comparing the two models, the Peleg model demonstrated a slightly better ability to represent the experimental data over a wider range of water activity, particularly across both the monolayer ($a_w \approx 0$–0.35) and multilayer ($a_w \approx 0.35$–0.6) regions. These regions correspond to moisture that is more strongly bound at low water activity and progressively less strongly bound as water activity increases. At higher water activity levels ($a_w > 0.6$), approaching the capillary condensation region (typically above $a_w \approx 0.9$), both models continued to provide reasonable agreement with the experimental data, although the Peleg model maintained slightly improved flexibility in capturing the curvature of the isotherm.

Both the Ferro-Fontan and Peleg models exhibited mean absolute percentage error (MAPE) values below 10% across all three temperatures investigated, indicating good predictive capability. Overall, while both models adequately describe the sorption behavior of FS, the Peleg model provides a more consistent representation across the full water activity range, particularly in capturing the transition between monolayer and multilayer moisture regimes. This further supports the use of the Peleg model for subsequent energetic analysis of moisture binding behavior.

3.1.2. Drying Test

The analysis using the Skyscan/Nrecon software V1.7.4.2 considered both the lateral area of the solid cylinder and the area provided by the two bases for the surface area, A mm^2, of the sample extrudate. Consequently, a correlation was established between the surface area of the sample (A, mm^2) and the MC on a dry basis (X, kg_{H2O}/kg_{TS}).

Upon plotting Krischer's curve for the samples, as shown in Figure 11, a clear constant drying rate period was observed. This behavior contrasted with earlier drying studies [17]. The different slopes of the curve can correspond to the different types of moisture. The interstitial moisture is the largest fraction of the bound moisture, at 37% of the total moisture for high solids sludges and significantly higher at 45–50% for septic tank samples. This was also observed in the stickiness determination of VIP samples at different temperatures of 60 °C and 80 °C [54]. The vicinal and internal moisture fractions are

similar for all the FS samples in the ranges 6–11% and 2–8% of the total moisture respectively. The moisture distribution from the drying tests is shown in Figure 12.

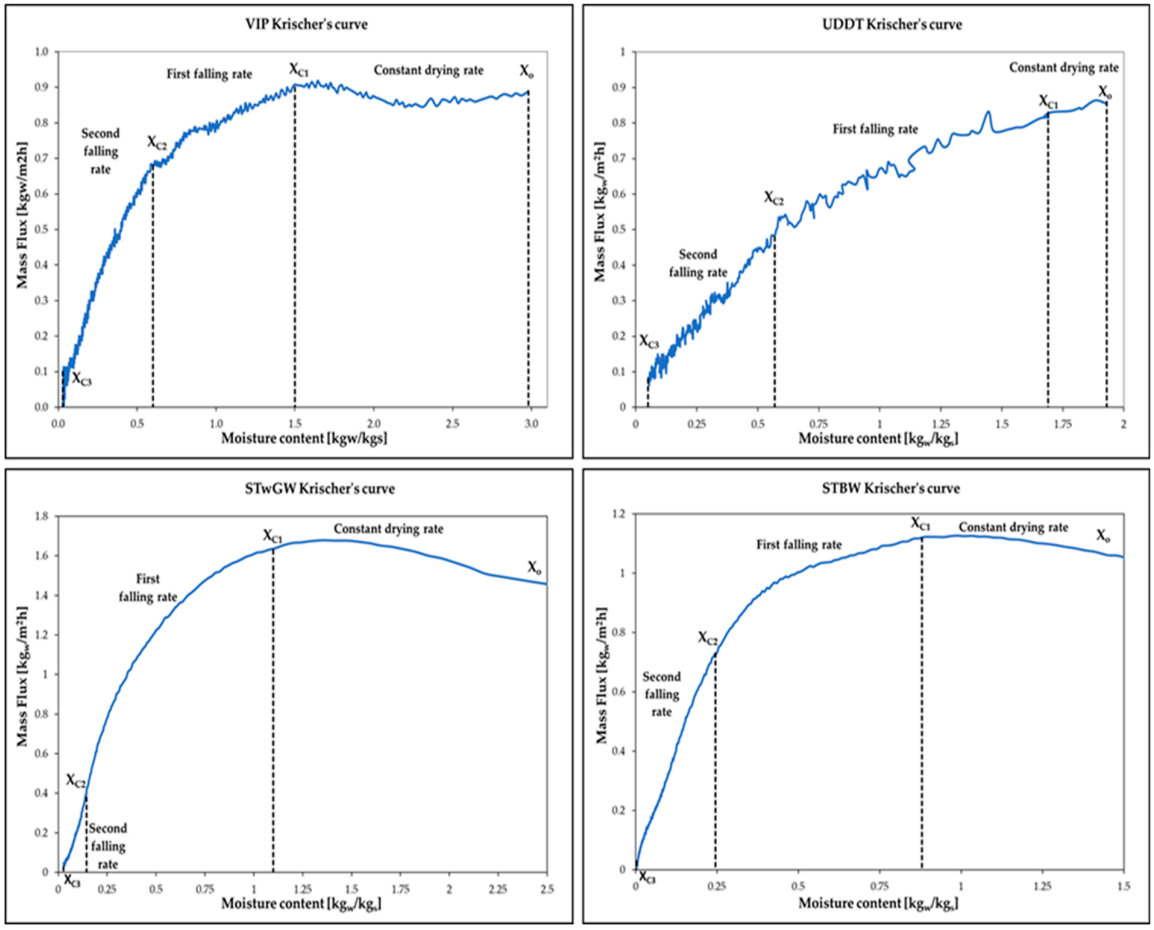

Figure 11. Krischer's drying curve of all FS samples, Mass flux ($kg_w/m^2.h$) Vs moisture content (kg_w/kg_s).

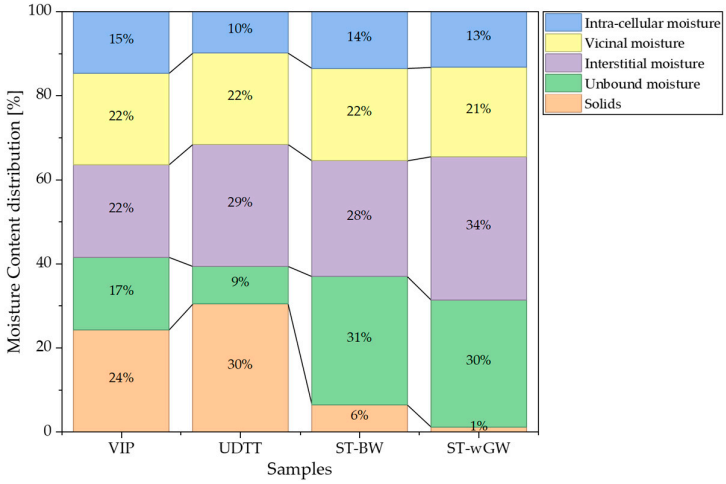

Figure 12. Moisture boundness from the drying test.

The measured drying data were used to determine the van Genuchten SWRC equation parameters using Origin software. The vG model was fitted to the dataset obtained from the low-temperature drying experiments, and the resulting fits are presented in Figure 13. The vG parameters provide insight into the capillary behavior of fecal sludge under unsaturated conditions.

In particular, the α parameter is associated with the inverse of the air-entry suction and therefore reflects the ease with which air penetrates the sludge matrix, providing an indication of pore size and capillary retention. The n parameter describes the pore size distribution and structural heterogeneity of the sludge. Together, these parameters enable characterization of the transition from capillary-dominated moisture retention at high moisture contents to adsorption-controlled moisture retention at lower moisture contents.

This transition is consistent with the moisture fraction framework identified in this study, where interstitial moisture is governed primarily by capillary forces, while vicinal and intracellular moisture are increasingly influenced by physicochemical interactions. The vG analysis therefore complements the energetic characterization by providing a capillary-based interpretation of moisture retention behavior in FS.

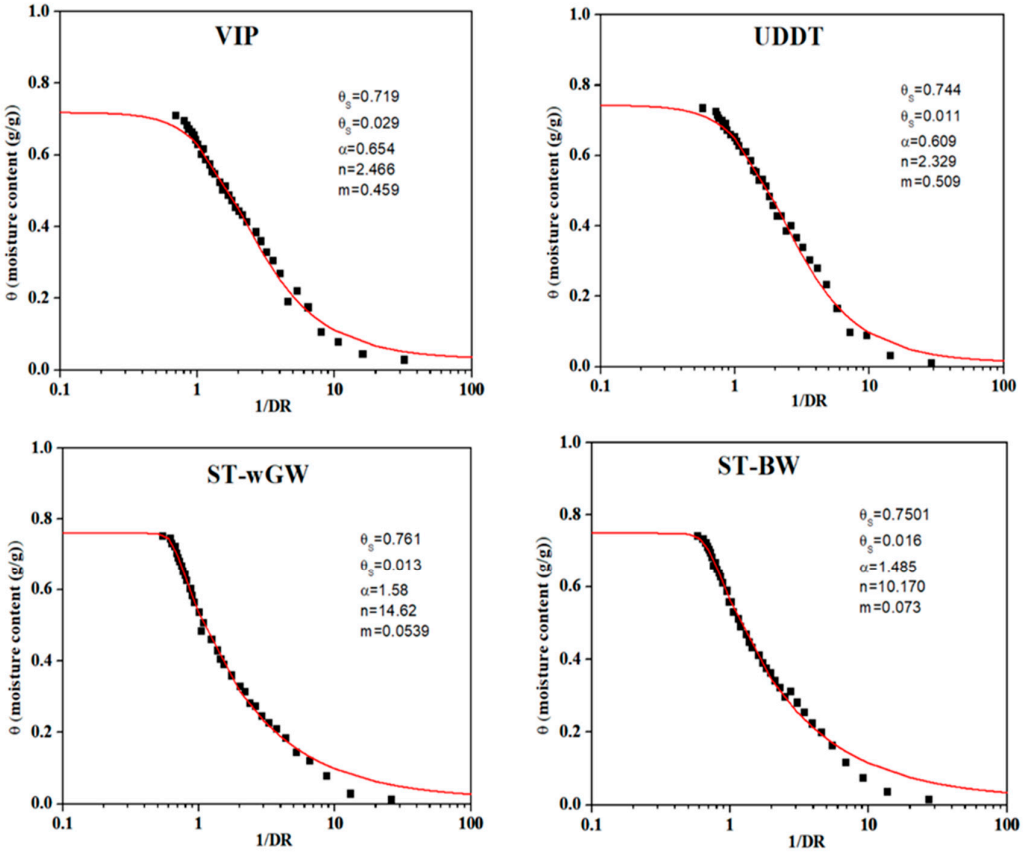

Figure 13. Application of van Genuchten model on different FSs.

The van Genuchten (vG) model provided a good representation of the drying data across all sludge types, with the fitted curves showing behavior comparable to that typically observed in plastic soils. The goodness of fit, as indicated by the coefficient of determination (R^2) values presented in Table 3, confirms that the vG model adequately captures the moisture retention behavior of fecal sludge under unsaturated conditions.

The VIP and UDDT samples exhibited slightly higher R^2 values compared to the ST-wGW and ST-BW samples, indicating a closer agreement between the model and

experimental data. This improved fit suggests a more homogeneous pore structure and more consistent capillary behavior in the VIP and UDDT sludges. In contrast, the relatively lower fit observed for the septic tank sludges may reflect greater heterogeneity arising from variations in organic content, particle size distribution, and the presence of grey water inputs.

The fitted vG parameters (α, m and n) further support this distinction. Similar parameter values obtained for VIP and UDDT samples indicate comparable capillary characteristics and pore structure, while the ST-wGW and ST-BW samples exhibit a different but internally consistent parameter grouping. These trends suggest that the moisture retention behavior of FS is influenced by its structural composition, which governs both capillary forces and the distribution of bound moisture within the sludge matrix. The higher α values observed in septic tank sludges (1.48–1.58) compared to VIP and UDDT samples (0.60–0.65) indicate lower air-entry suction and weaker capillary retention, consistent with their higher interstitial moisture fractions. Overall, the vG analysis demonstrates that FS exhibits soil-like unsaturated behavior, with moisture retention governed by capillary forces at higher moisture contents and progressively transitioning toward adsorption-controlled mechanisms at lower moisture contents.

Table 3. Details of the vG fitting parameters of the FS samples.

FS Sample	θ_s	θ_r	α	m	n	R^2
VIP	0.719	0.029	0.654	0.459	2.466	0.9576
UDDT	0.744	0.011	0.609	0.509	2.329	0.9696
ST-wGW	0.761	0.013	1.580	0.0539	14.620	0.9209
ST-BW	0.750	0.016	1.485	0.073	10.170	0.9356

3.1.3. NMR

In NMR, the area under the peak is proportional to the concentration of the moisture causing that peak. The CPMG experiment observed the relaxation of the transverse magnetization signal back to zero, followed by excitation to a maximum at $t = 0$, and the area under a peak decreased as the CPMG time increased. In other words, it measures the proportion of H nuclei that maintain magnetization at each time t. For a single nuclear environment within a pure substance, relaxation follows an exponential decay of the following form:

$$S = S_0 e^{-\frac{t}{T2}} \quad (6)$$

where S is the signal at time t, S_0 is the signal at time $t = 0$, t is the CPMG time, and $T2$ is the time constant for the transverse relaxation decay. From the range of $T2$ values, the different types of moisture were determined. The unbound moisture had a $T2$ value of a few seconds whereas the bound moisture had much lower $T2$ values. The true form of decay given by Equation (7) according to the Levenberg–Marquardt method, therefore, was as follows:

$$S(t) = A_1 e^{-\frac{t}{T21}} + A_2 e^{-\frac{t}{T22}} + A_3 e^{-\frac{t}{T23}} + \cdots + A_i e^{-\frac{t}{T2i}} \quad (7)$$

where $T21$, $T22$, $T23$ … $T2i$ are different $T2$ values and A_1, A_2, A_3 … A_i are the proportions of nuclei having the respective values of $T2$. The $T2$ relaxation decay data were fitted to Equation (7) and the T parameters were regressed by a simultaneous fit to all four samples. The amplitudes were weighted inversely to their magnitudes to give a better fit to low values in the exponential tails, as shown in Figure 14.

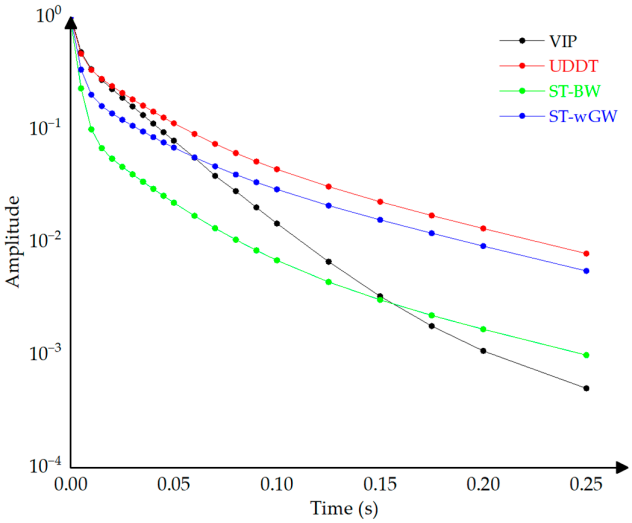

Figure 14. The T2 relaxation decay curves of the different FS samples.

From the multiexponential analysis, three peaks were extracted from the signals. To check whether the analysis gave consistent values for the exponential factors, their values were determined by fitting to each sample individually and then to all four samples simultaneously. The values were reasonably consistent. The three different water fractions were observed, in varying proportions, and it was observed that the smaller the *T*2 values, the tighter the binding of moisture and vice versa. While relaxation time distributions may overlap and do not uniquely define spatial moisture domains, the consistent grouping into three dominant relaxation regimes across all samples supports their correspondence to progressively constrained moisture states. The moisture distribution from the NMR data is provided in Figure 15.

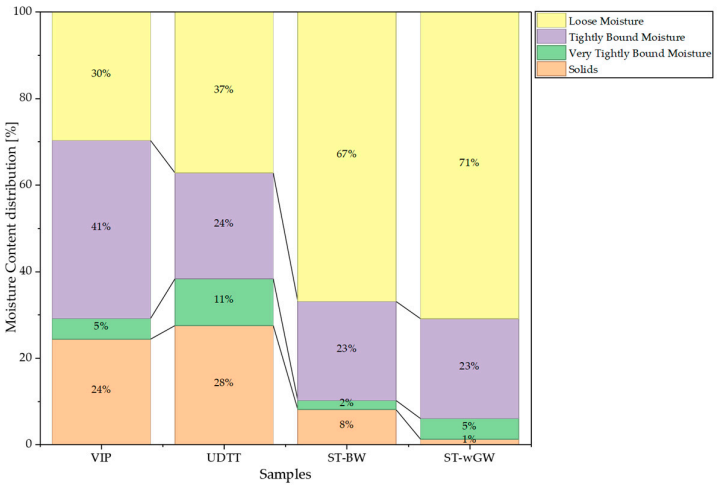

Figure 15. Moisture distribution from NMR experiments.

3.1.4. Comparative Assessment of Methods Used for Determining the Bound Moisture Fractions

Figure 16 compares the bound moisture fractions obtained from the three experimental techniques, low-T drying tests, MSI, and NMR, across the four FS samples. While the methods exhibit consistent directional trends, the figure clearly shows systematic and

method-dependent deviations (e.g., ~1–15% lower interstitial moisture in MSI relative to drying, and ±0–19% variation in NMR), reflecting differences in measurement principles rather than random variation. The drying test quantifies total removable moisture through gravimetric loss, MSI provides bulk proxy estimates based on spectral response, and NMR classifies moisture based on molecular mobility. As a result, fraction labels are not strictly equivalent across methods, particularly for intermediate moisture states.

Across all methods, interstitial moisture represents the dominant fraction of bound moisture, followed by vicinal moisture and finally intracellular moisture. For the VIP samples, the drying test estimated the interstitial moisture fraction at approximately 37–38% of total moisture, while MSI produced a similar value of about 36%. The NMR analysis produced a higher value of approximately 46%, reflecting the grouping of loosely bound moisture populations in the relaxation spectrum. MSI consistently reports lower interstitial values than drying, while NMR shows variable deviation, closely aligned in some cases (e.g., UDDT) but substantially lower or higher in others (e.g., ST-wGW and VIP). This variability reflects sensitivity to pore-scale distribution and mobility thresholds. The vicinal moisture fraction ranged from approximately 11–15% using MSI and drying methods, while intracellular moisture ranged from about 3–7%. The vicinal fraction is not directly comparable across methods. MSI reports higher values than drying, while NMR does not explicitly resolve this fraction since NMR characterizes moisture based on molecular mobility rather than spatial location within the sludge matrix. Consequently, NMR identifies two principal bound moisture populations, loosely bound and tightly bound water, rather than three discrete spatial fractions and the vicinal moisture is distributed between these two NMR populations, contributing partly to the loosely bound fraction together with interstitial moisture and partly to the tightly bound fraction together with intracellular moisture. This explains the systematic redistribution observed between NMR-derived values while still preserving the overall hierarchical structure of moisture binding. Accordingly, the differences between NMR and the other methods arise from the classification framework. Further, the intracellular fraction shows a consistent pattern across all systems, with NMR values systematically higher than those of both drying and MSI.

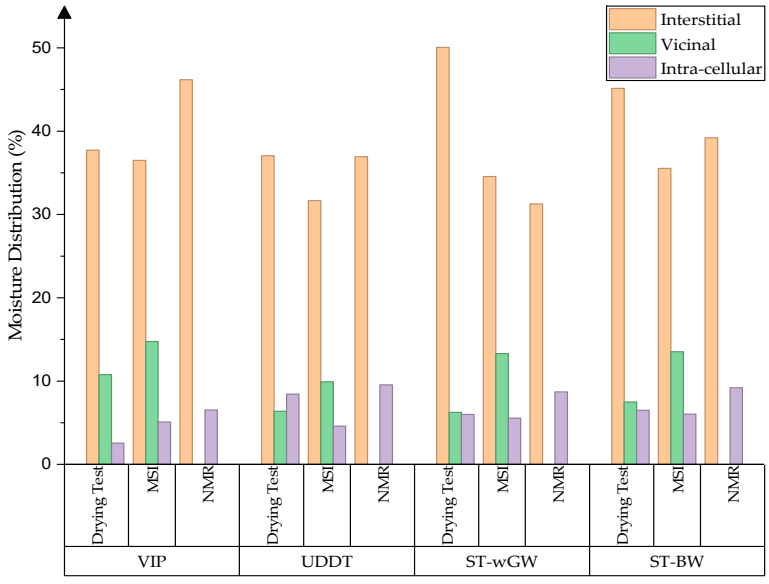

Figure 16. Comparative assessment of methods for bound moisture determination.

A comparable trend was observed for the UDDT samples, where interstitial moisture ranged from approximately 31–37% depending on the method. Vicinal moisture ranged from approximately 6–10%, while intracellular moisture remained within the range of about 4–9%. For the ST-wGW, the drying test produced the highest interstitial moisture estimate at approximately 50%, compared to about 34–35% obtained from MSI and NMR. The vicinal fraction varied from roughly 6–13%, and intracellular moisture ranged from approximately 5–9%. In the ST-BW samples, interstitial moisture ranged between approximately 31% (NMR) and 45% (drying test), with vicinal moisture from about 7–14% and intracellular moisture from approximately 6–9%. These differences, while substantial in magnitude, follow consistent method-specific bias patterns observed across all samples. Moisture fraction estimates are derived from processed datasets (drying curve averaging, model-fitted MSI isotherms, and NMR relaxation analysis). An uncertainty assessment based on error propagation, including contributions from image-based area estimation, indicates an overall uncertainty of approximately ±1–2% in the reported values. Conventional error bars are therefore not presented, as the values do not represent independent replicate measurements of the final fractions.

Despite these methodological differences, all three techniques produced consistent rank ordering of bound moisture fractions, with interstitial moisture representing the largest fraction across all FS types. The agreement between MSI, drying, and NMR in identifying interstitial moisture as the dominant fraction reduces the likelihood of a method-specific artefact, though the higher NMR estimates reflect its classification of loosely bound interstitial and vicinal populations together. Further, since the observed differences are driven by measurement constructs of the experiment approaches (gravimetric vs. proxy vs. molecular mobility), direct comparison of fractions, particularly unbound and vicinal, is therefore limited without conceptual harmonization.

3.2. Binding Energy Analysis

Binding energy was characterized through three independent approaches: drying kinetics from low-temperature convective drying, evaporation enthalpy from TGA-DSC, and net isosteric heat from MSI data. Together, these analyses provide insight into how moisture binding energy evolves as the sludge transitions from interstitial to vicinal and intracellular moisture regimes.

3.2.1. Kinetic Characteristics

The low-T drying test showed isothermal kinetic behavior consistent with the unreacted core model, in which the outer surface of the sample dries first and moisture diffuses outward through a progressively thickening dried layer. The heat transfer from the gas phase to the inside of the sample occurs by convection. The outer skin of the sample cylinder starts to dry first, and then the inner part. The moisture diffusion occurs through the pores of the dried outer surface. The unreacted core model has three rate-controlling steps [55].

(a) Kinetic control;
(b) Gas film control;
(c) Dried-layer control.

One of these three rate-controlling steps is the dominant of the three. The kinetic control is given by:

$$t = \tau\{1 - (1 - X)^{1/3}\} \quad (8)$$

where τ is the time required for the complete drying of the sample, X is the fractional conversion of drying and t is time.

X is given by:

$$X = \frac{m_0 - m}{m_0 - m_\infty} \quad (9)$$

where m_0 is the initial sample mass, m is the mass at time t and m_∞ is the sample mass after complete drying.

Diffusion of moisture through gas film controls is given by:

$$t = \tau X \quad (10)$$

The diffusion of moisture through dried-layer controls is given by:

$$t = \tau\left\{1 - 3(1 - X)^{\frac{2}{3}} + 2(1 - X)\right\} \quad (11)$$

The isothermal kinetic characteristic of the convective drying process is governed by the three rate-controlling steps which are compared (Figure 17) by applying the Equations (8), (10) and (11) and the relationship between the time and fractional conversion of drying is measured.

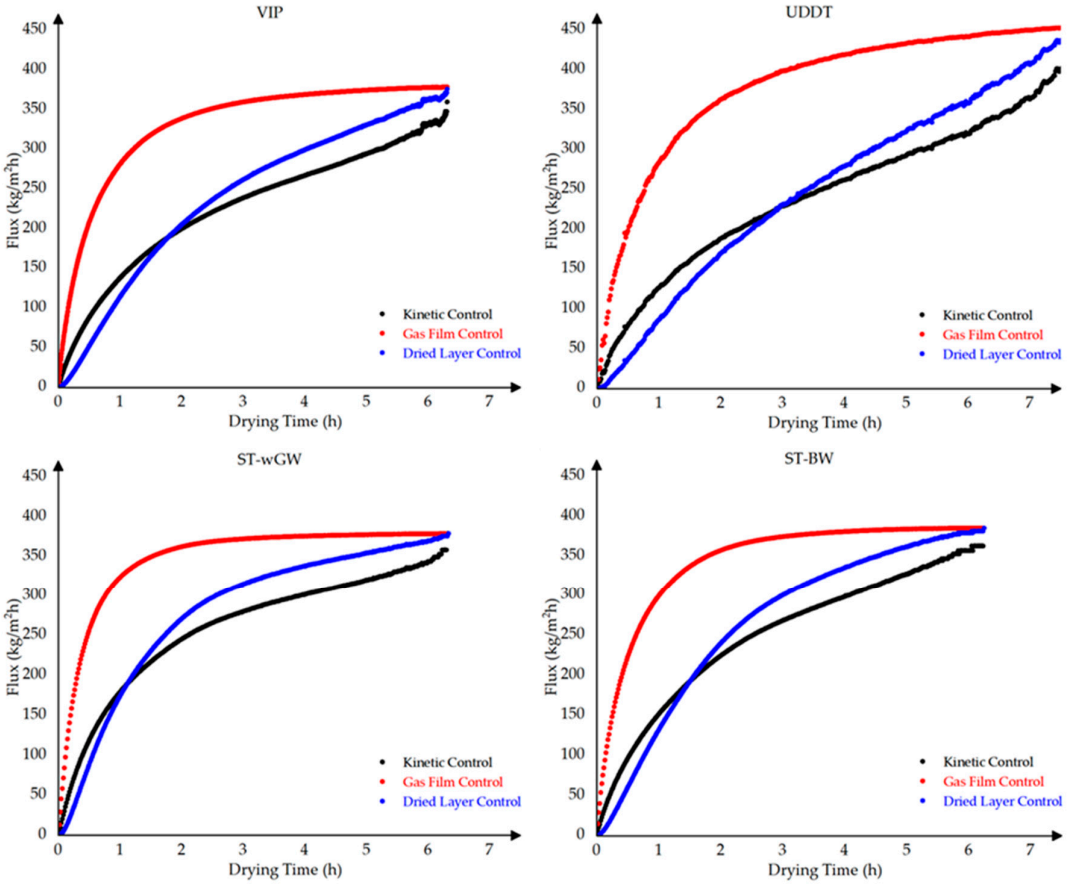

Figure 17. The rate-controlling steps of FS samples.

The comparison of the three rate-controlling models provides insight into the dominant transport mechanisms governing moisture removal from FS during low-temperature convective drying. Among the three models evaluated, the gas film control exhibited the lowest correlation coefficients (R^2 = 0.44–0.69), indicating that external mass transfer resistance between the drying air and the sludge surface was not the limiting mechanism. This suggests that the imposed airflow conditions and temperature were sufficient to maintain efficient moisture removal at the air–solid interface.

In contrast, both the kinetic control and dried-layer control models exhibited significantly higher correlations with the experimental data, as indicated in Table 4. The kinetic control model showed strong agreement across all sludge types (R^2 = 0.84–0.96), indicating that internal moisture migration within the sludge matrix plays a major role in governing drying behavior. This behavior is consistent with the heterogeneous biofloc structure of FS, where moisture must migrate through interconnected pore networks and gel-like microbial aggregates before reaching the evaporation surface.

Table 4. Comparison of three rate-controlling steps from low-T test for FS samples.

	Correlation R^2		
Samples	**Kinetic controls**	**Gas film controls**	**Dried-layer controls**
	Low-T Test	**Low-T Test**	**Low-T Test**
VIP	0.9273	0.5981	0.9249
UDDT	0.9597	0.6950	0.9766
ST-wGW	0.8444	0.4428	0.7983
ST-BW	0.9207	0.5370	0.8806

The dried-layer control model also exhibited similarly high correlations (R^2 = 0.80–0.98), particularly for the UDDT and VIP samples. This indicates that, as drying progresses, the formation of a partially dehydrated outer layer increasingly restricts moisture transport from the interior of the sample. The development of such a dried outer layer, often referred to as a "drying skin", creates an additional diffusion barrier that limits the movement of moisture vapor toward the evaporating surface. This phenomenon is commonly observed in drying of soft, porous materials and sludges where shrinkage and structural consolidation occur simultaneously with moisture loss.

The relative dominance of the kinetic and dried-layer mechanisms indicates that internal transport resistance, rather than external mass transfer, limits drying rate in FS. In the early drying stages, the kinetic control model suggests that moisture migration within the pore network governs the drying rate. As drying progresses and the outer layer consolidates, the dried-layer model provides a closer fit, consistent with the development of a diffusion-limiting surface layer. These stages are broadly consistent with the sequential removal of interstitial and vicinal moisture fractions, though direct assignment of drying periods to specific fractions requires further experimental validation.

This interpretation is consistent with the observed Krischer drying curves, where the first falling-rate period corresponds to capillary-driven removal of interstitial moisture, while the second falling-rate period reflects diffusion-limited removal of vicinal moisture. The increasing resistance to moisture transport observed in the later stages of drying therefore reflects the progressively stronger binding of moisture within the sludge matrix.

The co-dominance of kinetic and dried-layer mechanisms in all four FS types confirms that internal transport resistance, not external mass transfer, governs drying rate, consistent with the energetic hierarchy reported in Sections 3.2.2 and 3.2.3.

3.2.2. TGA-DSC Analysis

The TGA-DSC combined analysis allows us to evaluate the heat flow, temperature variation and mass loss rate of the sample. In Figure 18, a typical tests for pure water (a) and the FS sample are illustrated (b).

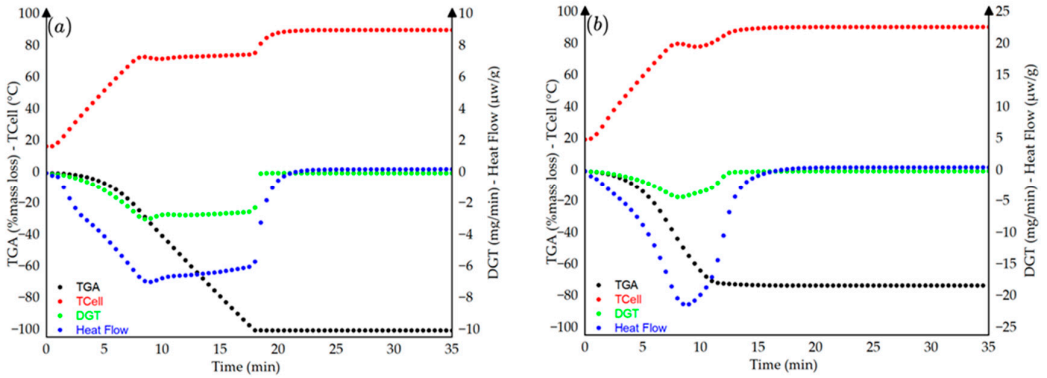

Figure 18. Experimental Results for Combined TGA-DSC Test for pure water (**a**) and VIP sample (**b**).

The sample weight (TGA), the calculated loss rate (DTG), the heat flow (DSC), and the reference cell temperature (Tcell) are shown in these figures as functions of time. In both graphs, the sample cell temperature initially increases from room temperature, exhibiting overshoots due to the temperature controller's regulation (Stage I). Once the surroundings reach the set temperature, the system stabilizes (Stage II). As the cell temperature rises, the sample mass decreases, indicating moisture loss. During Stage II of the TGA test for pure water (Figure 18(a)), the evaporation rate (DTG) remains nearly constant, reflecting a steady heat flow entirely dedicated to water evaporation. In contrast, for the VIP sludge test (Figure 18(b)), the constant DTG period is significantly shorter compared to the pure water test. As most of the moisture is removed, the process transitions to Stage III, where the evaporation rate declines rapidly. This transition is particularly abrupt for pure water (less than 2 min, Figure 18a), whereas in the VIP sludge test (Figure 18b), it occurs more gradually due to the complex moisture binding characteristics of the sludge.

From the obtained results, the specific enthalpy of moisture evaporation was calculated as follows. When the entire enthalpy flow is for moisture evaporation, the specific enthalpy or the evaporation heat of sludge moisture ΔH_s (kJ/kg) is given by Equation (12).

$$\Delta H_s = Q/m \tag{12}$$

where m is the drying rate, kg/s; Q is heat flow rate kJ/s and is given by Equation (13):

$$Q = Ah\,(T_{ref} - T_{cell}) \tag{13}$$

where A (m^2) is the heat transfer area; h (W/m^2·K) is the average heat transfer coefficient; and T_{ref} and T_{cell} are the reference temperature and cell temperature respectively. Ah is assumed to be constant for both pure water and the cell sample. $T_{ref} - T_{cell}$ can be derived from the DTA test.

The binding strength H_B (kJ/kg) is calculated using Equation (14) as follows:

$$H_B = H_s - H_W \tag{14}$$

where H_w is the heat of vaporization of pure water at 90 °C.

$\Delta H_s = \Delta H_p$ (the latent heat of water vaporization) when the moisture in the sample exhibits the same energy level as that of pure water, and this moisture is referred to as unbound moisture as it is accepted that unbound moisture has the same properties as that of pure water. Further, the solid particle–moisture binding is evident when $\Delta H_s > \Delta H_p$ and the difference is defined as the bond strength of the moisture. The higher the bond strength, the higher the required enthalpy to vaporize the moisture. The different energy levels indicated the different bond strengths, thereby depicting the different types of bound moisture [56]. Since the heat flow Q into the sample cell can be directly measured

through the DSC test, the pure water test is not needed in the TGA-DSC test (but it is useful to verify the equipment precision). The evaporation heat of moisture in sludge can be calculated directly through Equation (12), as well as the bond strength H_B in Equation (14). Figure 19 shows the experimental results of the FS samples. Higher binding energy denotes high enthalpy to separate from the solid particles, or more moisture boundness [57].

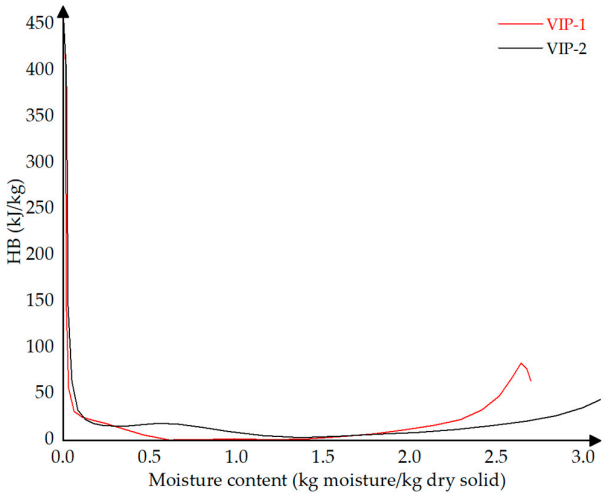

Figure 19. Bond strength of moisture in FS samples through TG-DSC test.

The excess enthalpy is consistent with increased binding of residual moisture, likely arising from a combination of capillary retention and surface adsorption effects [20]. The progressive increase in the binding strength observed across decreasing MC suggests that the bound moisture fractions are fundamentally differentiated by energy levels required for their removal rather than their spatial location alone. Accordingly, the interstitial moisture represents a low-energy bound state, whereas the vicinal and intracellular moisture corresponds to increasingly stable energetic configurations within the sludge matrix.

3.2.3. Net Isosteric Heat of Sorption (NIHS)

Net isosteric heat is a measure of the binding energy of moisture to the solid particles in a sludge and can show how moisture is bound at different moisture contents, corresponding to binding energies of the different moisture fractions. While the TGA-DSC cannot determine the vaporization energy at a defined temperature and provides accumulated average vaporization enthalpy, NIHS is defined at a specific temperature. NIHS was calculated at different MCs using the Clausius–Clapeyron equation and Ferro-Fantan and Peleg models that adequately fit the experimental data for the different samples at different temperatures. Figure 20 shows the relationship of the NIHS with MC (w.b) at 41.6 °C. The Ferro-Fontan model is limited to a water activity range of 0.1 to 0.9. During experimentation, this water activity range was achieved using the three MSI methods. The Peleg model offers a wider range of water activity of less than 0.95. However, it was observed that adequate points below 0.1 and above 0.9 but limited to 0.95 were necessary for a better estimation of model parameters by regression. These points were achieved using the water activity method during experimentation. Thus, a combination of points acquired from the saturated salt method would be necessary in the model parameter estimation.

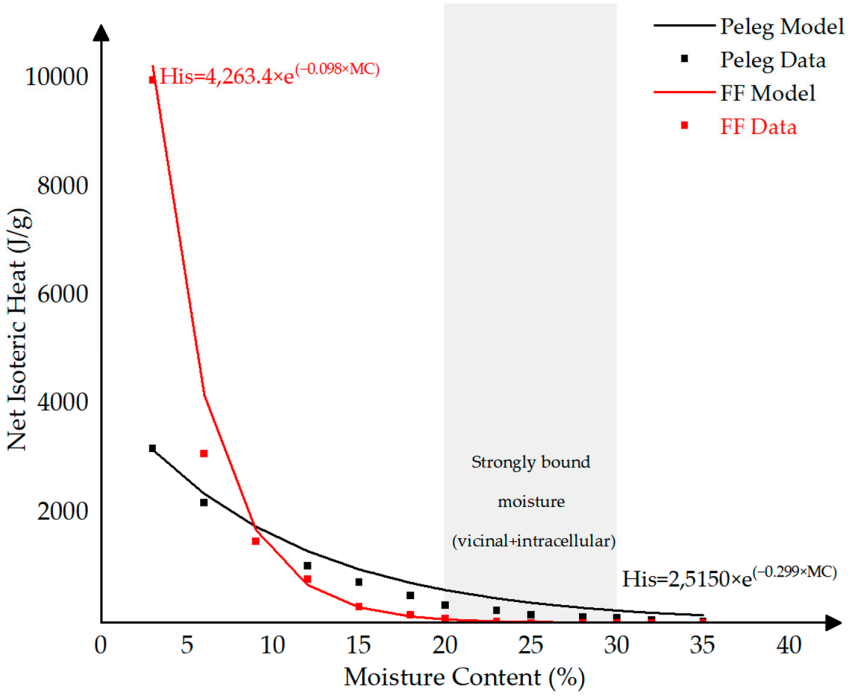

Figure 20. Variation of net isosteric heat (H_{is}) with moisture content for Ferro-Fontan and Peleg models, showing exponential decay behavior.

The net isosteric heat increased as the MC of the sample decreased. However, as the MC reaches 20% and 30% (w.b), the net isosteric heat became significant, which suggested that the NIHS was substantial for vicinal and internal moisture fractions. The higher NIHS with vicinal and internal moisture fractions was also consistent with van der Waals forces that attach to the sample surface to form a monolayer and with the water molecules in the multilayer. According to C. Bourgault et al., 2019 [28], the heat of evaporation is only significant up until 0.2 g water/g dry solids, which translates to an MC of 16.7% (w.b) in fresh feces at an average temperature of 25 °C. Although discrete energy values cannot be exclusively assigned to individual moisture fractions due to their overlapping transitions, the systematic escalation of NIHS and evaporation enthalpy with decreasing moisture content aligns consistently with the independently identified interstitial, vicinal and intracellular regimes.

The energetic hierarchy identified in this study provides a physical explanation for the progressive resistance of FS to moisture removal across different treatment processes. At higher moisture contents, interstitial moisture is associated with relatively low binding energies, consistent with capillary-dominated interactions. However, as moisture content decreases, the remaining water is increasingly associated with stronger physicochemical interactions, including adsorption onto particle surfaces, entrapment within structural networks and intracellular confinement. These structural networks are largely governed by extracellular polymeric substances (EPSs), which form a hydrated, gel-like matrix that regulates moisture retention behavior. The role of EPS in controlling sludge structure and stability has been independently characterized in a parallel study by the authors [20], where higher tightly bound EPS (TB-EPS) content was associated with increased structural integrity and moisture retention capacity. The trends observed in the present study are consistent with this structural interpretation. FSs such as ST-wGW and UDDT, which exhibit stronger persistence of bound moisture and a sharper increase in net isosteric heat at lower moisture contents, can be inferred to possess more developed EPS matrices, resulting in higher effective binding energy. In contrast, VIP samples exhibit comparatively

lower resistance to moisture removal, indicating weaker matrix-associated binding. The EPS matrix contributes to moisture binding through hydrogen bonding, electrostatic interactions, and physical entrapment within polymeric networks, thereby increasing the energy required for moisture removal. Accordingly, the increase in NIHS with decreasing moisture content reflects not only the transition between interstitial, vicinal, and intracellular moisture fractions but also the increasing dominance of EPS-mediated binding mechanisms within the sludge matrix.

This transition from interstitial to vicinal to intracellular moisture therefore represents a shift from capillary-controlled to structure- and interaction-controlled moisture retention. As the binding energy increases, moisture mobility becomes increasingly constrained, resulting in reduced efficiency of moisture removal irrespective of the method employed. While mechanical dewatering primarily overcomes capillary forces, thermal drying and other chemical processes must additionally overcome the higher energetic requirements associated with strongly bound moisture fractions. Consequently, these observations provide an energetic basis for understanding the residual moisture limits reported for different dewatering technologies applied to FS, particularly in explaining variability in achievable moisture reduction across treatment methods [4,10].

4. Conclusions

This study demonstrates that moisture in FS is organized as a continuum of bound states characterized by progressively increasing binding energies, corresponding to interstitial, vicinal, and intracellular moisture fractions. Across the investigated sludge types, interstitial moisture dominated bound moisture (33–50% of total moisture) and was governed by low-energy capillary interactions, while vicinal (9–15%) and intracellular fractions (3–9%) required progressively greater energy to remove. The van Genuchten model further indicated the behavior of moisture boundness of FS was similar to that of unsaturated soils.

Thermal and thermodynamic analyses (TGA-DSC and NIHS) confirmed that binding energy increases with decreasing moisture content, reflecting a transition from capillary-controlled to structure-controlled moisture retention. This transition, evident through the falling rate periods and the sharp increase in NIHS at 20–30% moisture content, corresponds to the dominance of strongly bound vicinal and intracellular moisture. This energetic transition is intrinsically linked to the structural characteristics of the sludge matrix, particularly the presence of EPSs, which form a hydrated network governing moisture retention.

The three experimental approaches—sorption isotherms, low-temperature drying, and TGA-DSC—characterized moisture binding through complementary perspectives and the consistent rank ordering of moisture fractions across all three methods supports the robustness of the identified hierarchy and reduces the likelihood of method-specific artefacts, though the different physical bases of each method preclude direct quantitative equivalence. Across sanitation systems, the observed differences in binding energy behavior indicate that septic tank and UDDT sludges exhibit stronger moisture retention environments compared to VIP sludges, consistent with more developed matrix structures. These differences suggest that variations in EPS composition contribute directly to binding energy behavior and residual moisture limits.

The findings provide a thermodynamic basis for understanding residual moisture limits in FS treatment. Elevated binding energies associated with vicinal and intracellular moisture indicate that improving dewaterability requires approaches that modify sludge microstructure. In practical terms, for FS with high interstitial moisture content (e.g., >45% as in septic tank sludges), approaches that modify sludge microstructure, particularly through disruption of EPS networks, may be more effective than increasing applied

mechanical stress alone, as EPS-mediated binding governs the retention of strongly bound moisture fractions.

Author Contributions: A.K.R.S.: Conceptualization, Methodology, Investigation, Formal analysis, Visualization, Writing—original draft; L.M.: Methodology, Investigation, Formal analysis, Visualization, Writing—original draft; S.L.P.-A.: Investigation, Formal analysis, Visualization, Writing—original draft; A.L.: Methodology, Writing—review and editing; J.P.: Conceptualization, Methodology, Writing—review and editing; S.S.: Conceptualization, Methodology, Writing—review and editing. All authors have read and agreed to the published version of the manuscript.

Funding: This research was funded by the Bill and Melinda Gates Foundation, grant number OPP1170678 through Water Research Commission, South Africa. The authors also acknowledge the Fund for Scientific Research Belgium (F.R.S.–FNRS) for funding this research through grant T.0159.20-PDR.

Institutional Review Board Statement: The study was conducted in accordance with the ethical clearance obtained from the Biomedical Research Ethics Administration (BREC) from the University of KwaZulu-Natal (protocol reference number: BREC/00002194/2020).

Informed Consent Statement: Not applicable.

Data Availability Statement: The data presented in this study are available on request from the corresponding author due to ethical reasons.

Acknowledgments: The authors gratefully acknowledge the WASH R&D Centre and the Department of Chemical Engineering at the University of KwaZulu-Natal for institutional support and laboratory facilities. The authors sincerely thank Angélique Léonard, Alexandre Leonard and Erwan Plougonven at the Chemical Engineering Research Unit (PEPs), University of Liège, for their guidance and support in the moisture sorption and low-temperature convective drying experiments. The authors also gratefully acknowledge the invaluable support provided by the staff of the Chemical Engineering Hall at the University of Liège. The authors also acknowledge Joel Loveridge at Swansea University for assistance with the nuclear magnetic resonance measurements and Avinash Ramsaroop at the Thermal Analysis Laboratory, Durban University of Technology, for support with the TGA–DSC analyses. The authors further thank Biswajit Panda (Interdisciplinary Centre for Water Research, Indian Institute of Science, Bengaluru) for his valuable insights and discussions on the application of the van Genuchten model. Their technical expertise and insightful discussions contributed significantly to the completion of this work.

Conflicts of Interest: The authors declare no conflicts of interest.

Abbreviations

The following abbreviations are used in this manuscript:

DVS	Dynamic Vapor Sorption
FS	Fecal Sludge
MSI	Moisture Sorption Isotherm
NMR	Nuclear Magnetic Resonance
ST-BW	Septic Tank—Black Water Only
ST-wGW	Septic Tank—with Grey Water Also
SWCC	Soil Water Characteristic Curve
TGA-DSC	Thermogravimetric Analysis–Differential Scanning Calorimetry
UDDT	Urine-Diverting Dehydrating Toilet
VIP	Ventilated Pit Latrine
WA	Water Activity

References

1. Diener, S.; Semiyaga, S.; Niwagaba, C.B.; Muspratt, A.M.; Gning, J.B.; Mbéguéré, M.; Ennin, J.E.; Zurbrugg, C.; Strande, L. A value proposition: Resource recovery from faecal sludge—Can it be the driver for improved sanitation? *Resour. Conserv. Recycl.* **2014**, *88*, 32–38. https://doi.org/10.1016/j.resconrec.2014.04.005.
2. Mallory, A.; Holm, R.; Parker, A. A Review of the Financial Value of Faecal Sludge Reuse in Low-Income Countries. *Sustainability* **2020**, *12*, 8334. https://doi.org/10.3390/su12208334.
3. Muoghalu, C.; Semiyaga, S.; Manga, M. Faecal sludge emptying in Sub-Saharan Africa, South and Southeast Asia: A systematic review of emptying technology choices, challenges, and improvement initiatives. *Front. Environ. Sci.* **2023**, *11*, 1097716. https://doi.org/10.3389/fenvs.2023.1097716.
4. Cunningham, M.; Gold, M.; Strande, L. Literature Review: Slow pyrolysis of faecal sludge. 2016. P. 85. Available online: https://www.dora.lib4ri.ch/eawag/item/eawag:14834 (accessed on 17 May 2026).
5. Basamykina, A.; Kharlamova, M.; Mada, S.Y. Dewatering as a Primary Treatment of Faecal Sludge in Individual Residential Sector (a Technologies Review). In *E3S Web of Conferences*; EDP Sciences: Les Ulis, France, 2020. https://doi.org/10.1051/e3sconf/202016902008.
6. Schaum, C.; Lux, J. Sewage Sludge Dewatering and Drying. Available online: https://api.semanticscholar.org/CorpusID:133599980 (accessed on 17 May 2026).
7. Gold, M.; Ddiba, D.I.W.; Seck, A.; Sekigongo, P.; Diene, A.; Diaw, S.; Niang, S.; Niwagaba, C.; Strande, L. Faecal sludge as a solid industrial fuel: A pilot-scale study. *J. Water Sanit. Hyg. Dev.* **2017**, *7*, 243–251. https://doi.org/10.2166/washdev.2017.089.
8. To, V.H.P.; Nguyen, T.V.; Vigneswaran, S.; Ngo, H.H. A review on sludge dewatering indices. *Water Sci. Technol.* **2016**, *74*, 1–16. https://doi.org/10.2166/wst.2016.102.
9. Novak, J.T. Dewatering of Sewage Sludge. *Dry. Technol.* **2006**, *24*, 1257–1262. https://doi.org/10.1080/07373930600840419.
10. Wu, B.; Dai, X.; Chai, X. Critical review on dewatering of sewage sludge: Influential mechanism, conditioning technologies and implications to sludge re-utilizations. *Water Res.* **2020**, *180*, 115912. https://doi.org/10.1016/j.watres.2020.115912.
11. Möller, U.K. Water Binding. *In Sludge Characteristics and Behavior*; Springer: Berlin/Heidelberg, Germany, 1983; pp. 182–194.
12. Smollen, M. Categories of Moisture Content and Dewatering Characteristics of Biological Sludges. In Proceedings of the Fourth World Filtration Congress, Ostend, Belgium, 19–25 April 1986; Volume 14, pp. 35–41.
13. Smollen, M. Moisture retention characteristics and volume reduction of municipal sludges. *Water SA* **1988**, *14*, 25–28.
14. Colin, F.; Gazbar, S. Distribution of water in sludges in relation to their mechanical dewatering. *Water Res.* **1995**, *29*, 2000–2005. https://doi.org/10.1016/0043-1354(94)00274-b.
15. Kopp, J.; Dichtl, N. Influence of the free water content on the dewaterability of sewage sludges. *Water Sci. Technol.* **2001**, *44*, 177–183. https://doi.org/10.2166/wst.2001.0613.
16. Kopp, J.; Dichtl, N. Prediction of full-scale dewatering results by determining the water distribution of sewage sludges. *Water Sci. Technol.* **2000**, *42*, 141–149. https://doi.org/10.2166/wst.2000.0191.
17. Vaxelaire, J.; Cézac, P. Moisture distribution in activated sludges: A review. *Water Res.* **2004**, *38*, 2215–2230. https://doi.org/10.1016/j.watres.2004.02.021.
18. Kumar, A.; Suryakumar, R.; Mercer, E.; Pocock, J.; Septien, S. Determination of unbound-bound moisture interface of faecal sludges from different on-site sanitation systems. *Heliyon* **2024**. https://doi.org/10.1016/j.heliyon.2025.e42091
19. Erdincler, A.; Vesilind, P.A. Effect of Sludge Water Distribution on the Liquid–Solid Separation of a Biological Sludge. *J. Environ. Sci. Health Part A Toxic/Hazard. Subst. Environ. Eng.* **2003**, *38*, 2391–2400. https://doi.org/10.1081/ese-120023439.
20. Rayavellore Suryakumar, A.K.; Parra-Angarita, S.L.; Léonard, A.; Pocock, J.; Septien, S. Mechanical Properties of Faecal Sludge and Its Influence on Moisture Retention. ChemEngineering 2025, 9, 2. https://doi.org/10.3390/chemengineering9010002
21. Fontan, C.F.; Chirife, J.; Sancho, E.; Iglesias, H.A. Analysis of a Model for Water Sorption Phenomena in Foods. *J. Food Sci.* **1982**, *47*, 1590–1594. https://doi.org/10.1111/j.1365-2621.1982.tb04989.x.
22. Kurniawan, Y.R.; Purwanto, Y.A.; Purwanti, N.; Budijanto, S. Measurement of Moisture Sorption Isotherm by DVS Hydrosorb. *IOP Conf. Ser. Earth Environ. Sci.* **2018**, *147*, 012017.
23. Vesilind, P.A. The role of water in sludge dewatering. *Water Environ. Res.* **1994**, *66*, 4–11. https://doi.org/10.2175/wer.66.1.2.
24. Vesilind, P.; Hsu, C. Limits of sludge dewaterability. *Water Sci. Technol.* **1997**, *36*, 87–91. https://doi.org/10.2166/wst.1997.0397.
25. Fontana, A.J.; Carter, B.P. Measurement of Water Activity, Moisture Sorption Isotherm, and Moisture Content of Foods. In Water Activity in Foods: Fundamentals and Applications, 2nd ed.; Barbosa-Cánovas, G.V., Fontana, A.J., Schmidt, S.J., Labuza, T.P., Eds.; Wiley: Hoboken, NJ, USA, 2020; pp. 207–226.

26. Arlabosse, P.; Rodier, E.; Ferrasse, J.H.; Chavez, S.; Lecomte, D. Comparison Between Static and Dynamic Methods for Sorption Isotherm Measurements. *Dry. Technol.* **2003**, *21*, 479–497. https://doi.org/10.1081/drt-120018458.
27. Simo-Tagne, M.; Bennamoun, L.; Léonard, A.; Rogaume, Y. Determination and modeling of the isotherms of adsorption/desorption and thermodynamic properties of obeche and lotofa using nelson's sorption model. *Heat Mass Transf. Und Stoffuebertragung* **2019**, *55*, 2185–2197. https://doi.org/10.1007/s00231-019-02577-2.
28. Bourgault, C.; Lessard, P.; Remington, C.; Dorea, C.C. Experimental Determination of Moisture Sorption Isotherm of Fecal Sludge. *Water* **2019**, *11*, 303. https://doi.org/10.3390/w11020303.
29. Ruiz-López, I.I.; Herman-Lara, E. Statistical Indices for the Selection of Food Sorption Isotherm Models. *Dry. Technol.* **2009**, *27*, 726–738. https://doi.org/10.1080/07373930902827932.
30. Leonard, A.; Blacher, S.; Marchot, P.; Crine, M. Use of X-ray microtomography to follow the convective heat drying of wastewater sludges. *Dry. Technol.* **2002**, *20*, 1053–1069. https://doi.org/10.1081/drt-120004013.
31. Yu, W.; Li, P.S. Determine the Moisture Distribution in Sewage Sludge by Drying Differential. *Appl. Mech. Mater.* **2014**, *665*, 404–407. https://doi.org/10.4028/www.scientific.net/amm.665.404.
32. de Lima, A.G.B.; Delgado, J.M.P.Q.; Neto, S.R.F.; Franco, C.M.R. Intermittent drying: Fundamentals, modeling and applications. In *Drying and Energy Technologies*; Springer International Publishing: Cham, Switzerland, 2015; pp. 19–41.
33. Tsang, K.R.; Vesilind, P.A. Moisture Distribution in Sludges. *Water Sci. Technol.* **1990**, *22*, 135–142. https://doi.org/10.2166/wst.1990.0108.
34. Pan, H.; Qing, Y.; Pei-Yong, L. Direct and indirect measurement of soil suction in the laboratory. *Electron. J. Geotech. Eng.* **2010**, *15*, 1–14.
35. Léonard, A. Étude du Séchage Convectif de Boues de Station D'épuration—Suivi de la Texture par Microtomographie à Rayons x. PhD Thesis, Universite de Liege, Liege, Belgium, 2002.
36. Nielsen, R.V.; Jensen, M.; Duus, S.A.C.; Christensen, M.L. Critical moisture point of sludge and its link to vapour sorption and dewatering. *Chemosphere* **2019**, *236*, 124299. https://doi.org/10.1016/j.chemosphere.2019.07.030.
37. Mujumdar, A.S.; Devahastin, S. *Fundamental Principles of Drying*; Exergex: Brossard, QC, Canada 2011.
38. Lee, D.J.; Lai, J.Y.; Mujumdar, A.S. Moisture Distribution and Dewatering Efficiency for Wet Materials. *Dry. Technol.* **2006**, *24*, 1201–1208. https://doi.org/10.1080/07373930600838041.
39. Léonard, A.; Blacher, S.; Marchot, P.; Pirard, J.P.; Crine, M. Measurement of Shrinkage and Cracks Associated to Convective Drying of Soft Materials by X-ray Microtomography. *Dry. Technol.* **2004**, *22*, 1695–1708. https://doi.org/10.1081/drt-200025629.
40. Léonard, A.; Blacher, S.; Marchot, P.; Pirard, J.; Crine, M. Image analysis of X-ray microtomograms of soft materials during convective drying: 3D measurements. *J. Microsc.* **2005**, *218*, 247–252. https://doi.org/10.1111/j.1365-2818.2005.01485.x.
41. Fredlund, D.; Xing, A. Equations for the soil-water characteristic curve. *Can. Geotech. J.* **1994**, *31*, 521–532. https://doi.org/10.1139/t94-061.
42. Genuchten, V.M. A closed-form equation for predicting the hydraulic conductivity of unsaturated soils. *Soil Sci. Soc. Am. J.* **1980**, *44*, 892–898.
43. Rahimi, A.; Rahardjo, H.; Leong, E.-C. Effect of range of soil–water characteristic curve measurements on estimation of permeability function. *Eng. Geol.* **2015**, *185*, 96–104. https://doi.org/10.1016/j.enggeo.2014.11.017.
44. Liu, J.; Yin, B.; Tang, W.; Li, J.; Liu, Y.; Zhao, H. An extended model based on the general Van Genuchten model for the "wetting" process of GMZ Na-bentonite subjected to alkali-heat treatment. *Constr. Build. Mater.* **2023**, *392*, 131935. https://doi.org/10.1016/j.conbuildmat.2023.131935.
45. Liukkonen, M.; Nikolskaya, E.; Selin, J.; Hiltunen, Y. Water Content Analysis of Sludge using NMR Relaxation Data and Independent Component Analysis. In Proceedings of the 2016 9th EUROSIM Congress on Modelling and Simulation (Eurosim 2016), Oulu, Finland, 12–16 September 2016; pp. 317–320.
46. Mao, F.; Zhao, Y.; Zhang, Y.; Chen, Z.; Yin, L. Measurement and Modelling of Moisture Distribution and Water Binding Energy of Dredged Sludge. *Water* **2020**, *12*, 3395. https://doi.org/10.3390/w12123395.
47. Okada, K.; Hayashi, Y.; Kumada, S.; Onuki, Y. Nondestructive Investigation of the Agglomeration Process for Nanosuspensions via NMR Relaxation of Water Molecules. *Eur. J. Pharm. Sci.* **2021**, *164*, 105908. https://doi.org/10.1016/j.ejps.2021.105908.
48. Ferrasse, J.-H.; Lecomte, D. Simultaneous heat-flow differential calorimetry and thermogravimetry for fast determination of sorption isotherms and heat of sorption in environmental or food engineering. *Chem. Eng. Sci.* **2004**, *59*, 1365–1376. https://doi.org/10.1016/j.ces.2004.01.002.

49. Ferrasse, J.H.; Arlabosse, P.; Lecomte, D.; Schwartzentruber, J.;. Apport du couplage d'une thermobalance gravimétrique et d'un analyseur calorimétrique différentiel pour la mesure de l'activité de l'eau dans un mélange liquide solide. Entropie 2000, 224–225, 80–85 https://hal.science/hal-01847607v1
50. Lin, F.; Li, J.-G.; Chai, X.-S.; Zhang, Z.-B.; Liu, M. Determination of water distribution in sludge by a multiple headspace extraction analytical technique. *J. Chromatogr. A* **2020**, *1628*, 461449. https://doi.org/10.1016/j.chroma.2020.461449.
51. Deng, W.; Li, X.; Yan, J.; Wang, F.; Chi, Y.; Cen, K. Moisture distribution in sludges based on different testing methods. *J. Environ. Sci.* **2011**, *23*, 875–880. https://doi.org/10.1016/s1001-0742(10)60518-9.
52. Zhang, W.; Xu, Y.; Dong, B.; Dai, X. Characterizing the sludge moisture distribution during anaerobic digestion process through various approaches. *Sci. Total. Environ.* **2019**, *675*, 184–191. https://doi.org/10.1016/j.scitotenv.2019.04.095.
53. Bougayr, E.H.; Lakhal, E.K.; Idlimam, A.; Lamharrar, A.; Kouhila, M.; Berroug, F. Experimental study of hygroscopic equilibrium and thermodynamic properties of sewage sludge. *Appl. Therm. Eng.* **2018**, *143*, 521–531. https://doi.org/10.1016/j.applthermaleng.2018.07.048.
54. Mupinga, R.T.; Mercer, E.; Suryakumar, A.R.; Pocock, J.; Septien, S. Insight into the stickiness of faecal sludge from dry sanitation technologies: A path toward sustainable and efficient FSM via thermal processes. *Results Eng.* **2025**, *26*, 105453. https://doi.org/10.1016/j.rineng.2025.105453.
55. Qian, J.; Yoon, Y.W.; Youn, P.S.; Kim, J.H.; Choi, D.S.; Choi, J.-H.; Choi, Y.C.; Jung, B. Drying characteristics of sewage sludge. *Korean J. Chem. Eng.* **2011**, *28*, 1636–1640. https://doi.org/10.1007/s11814-011-0009-5.
56. Chen, G.W.; Hung, W.T.; Chang, I.L.; Lee, S.F.; Lee, D.J. Continuous classification of moisture content in waste activated sludges. *J. Environ. Eng.* **1997**, *123*, 253–258.
57. Chu, C.; Lee, D. Structural analysis of sludge flocs. *Adv. Powder Technol.* **2004**, *15*, 515–532. https://doi.org/10.1163/1568552042000246.